Coordination Chemistry Reviews 279 (2014) 141–160

Contents lists available at ScienceDirect

Coordination Chemistry Reviews

journal homepage: www.elsevier.com/locate/ccr

Review

Entangled structures in polyoxometalate-based coordination polymers

Wen-Wen He[a], Shun-Li Li[b], Hong-Ying Zang[a], Guang-Sheng Yang[a], Shu-Ran Zhang[a], Zhong-Min Su[a,*], Ya-Qian Lan[a,b,**]

[a] Institute of Functional Material Chemistry, Key Lab of Polyoxometalate Science of Ministry of Education, Faculty of Chemistry, Northeast Normal University, Changchun 130024, PR China
[b] Jiangsu Key Laboratory of Biofunctional Materials, School of Chemistry and Materials Science, Nanjing Normal University, Nanjing 210023, PR China

Contents

ARTICLE INFO

Article history:
Received 18 October 2013
Accepted 19 March 2014
Available online 3 April 2014

Keywords:
POM-based coordination polymer
Interpenetration

ABSTRACT

Polyoxometalates (POMs) have attracted a lot of interest due to their novel structure characteristics and various connection modes. POM-based coordination polymers with entangled structures, an indispensable branch of entangled networks, take advantage of the features of POMs, and have received increasing attention. Much effort has been devoted over the past few decades toward their preparation and the analysis of their unusual entangled topology. In this review, we will summarize a number of examples of POM-based coordination polymer that have been described according to their different entangled characteristics. Different concepts, such as interpenetration, polycatenation, polyrotaxane,

* Corresponding author. Fax: +86 431 85684009.
** Corresponding author. Fax: +86 25 85891051.
E-mail addresses: zmsu@nenu.edu.cn (Z.-M. Su), yqlan@njnu.edu.cn (Y.-Q. Lan).

http://dx.doi.org/10.1016/j.ccr.2014.03.022
0010-8545/© 2014 Elsevier B.V. All rights reserved.

Polycatenation
Polyrotaxane
Poly*pseudo*-rotaxane
Self-penetration

poly*pseudo*-rotaxane and self-penetration, are employed to describe the various types of POM-based coordination polymers with entangled structures. In addition, we further classify POM-based coordination polymers with entangled structures based on the dimensionalities of the individual motifs and the roles of the POMs. Combining the advantages of the attractive potential applications of the POMs and structure diversities of the entangled frameworks, the investigation of POM-based coordination polymers with entangled structures will be a sustainable research field in coordination chemistry.

© 2014 Elsevier B.V. All rights reserved.

1. Introduction

Polyoxometalates (POMs) are early transition metal oxyanionic clusters that show a wide variety of interesting structural motifs; their diversity allows for applications in different fields such as catalysis, medicine, biology and materials science [1,2]. POM-based coordination polymers (also written as POM-based metal-organic frameworks (MOFs) in some articles) are a series of hybrid organic–inorganic materials composed of polyoxometalates and different metal-organic units [3]. Over a thousand articles related to POM-based coordination polymers have been documented by the Web of Knowledge to date [4–6] (Scheme 1). Among studies of the potential applications ranging from catalysis and adsorption of POM-based coordination polymers, the architecture and topology of entangled POM-based coordination polymers have been of particular interest [7–9]. The topological analysis of multitudinous networks is not only an important tool for simplifying complicated compounds, it also plays an instructive role in the rational design of targetable functional materials with desirable properties [10–13]. In short, topological studies make a significant contribution toward the controllable synthesis and property studies of POMs and POM-based coordination polymers.

Entangled systems, as one of the major themes of supramolecular chemistry, are comprised of individual motifs forming, via interlocking or interweaving, a periodic architecture that is infinite in at least one dimension [14,15]. In addition to the common phenomenon of interpenetration, particular attention has been devoted to characterizing these extended entanglements. The phenomenon of mechanical interlocking, which is typical of molecular structures such as catenanes, rotaxanes and knots, has been studied extensively [16–22]. Furthermore, most of these species can be considered regularly repeating infinite versions of the finite molecular motifs, and can lead to synthetic supramolecular arrays with a variety of structural features (Scheme 2). Many topologically interesting entangled structures have been discussed in comprehensive reviews by Batten, Robson and Ciani [14–16,23,24]. However, a review on the progress of POM-based coordination polymers with entangled structures has not yet appeared.

POMs in the framework may exhibit numerous connecting modes, which have a great effect on the formation of the final structure [25–29]. When analyzing different roles of POMs in the entangled POM-based coordination polymers, we separate them into two categories. (I) Systems with POMs as linkers (from the perspective of mathematical theory), in which POMs serve as versatile inorganic linkages by providing terminal and/or bridging oxygen atoms to connect with different metal-organic units to construct POM-based multifunctional hybrid materials. (II) Systems with POMs as templates, where POMs, as a unique class of inorganic metal oxide clusters, have been regarded as excellent candidates for templates to obtain POM-based coordination polymers due to their tunable size and high negative charge.

In this review, we will investigate examples of POM-based coordination polymers in the literature and describe their different entangled characteristics. Additionally, we further classify POM-based coordination polymers with entangled structures based on the dimensionalities of the individual motifs and the roles of the POMs, because inclusion of POMs in the assembly has a significant impact on the formation of the entangled structure.

In the first section, we will briefly review interpenetration-involved POM-based coordination polymers in an attempt to accomplish an initial classification of the different interweaving and interlocking aspects (2D layer or 3D network). Later sections use different concepts, such as polycatenation, polyrotaxane, poly*pseudo*-rotaxane and self-penetration, to describe other types of entangled structures in POM-based coordination polymers (Scheme 3) [14,15,24].

2. Interpenetration in POM-based coordination polymers

Among the different types of entangled systems, interpenetration is the most common form of entanglement and has been extensively studied over the past decade. The longer, flexible ligands usually yield compounds with high connectivity and larger voids, but these kinds of compound are always unstable. Thus, interpenetration reasonably occurs to reduce pore space in order to decrease the instability. It is almost impossible not to mention polycatenation when describing interpenetration because of their close relationship [14,23].

Generally, for interpenetration systems: (1) all individual motifs with identical topologies are usually extended infinitely into 2D or 3D networks; (2) the number of interpenetrated motifs is finite; (3) the resulting dimensionality equals the number of component motifs; (4) each single network is interlaced with all the other ones to create the final structure. Conversely, for polycatenation: (1) the motifs can be 0D, 1D (with closed circuits) or 2D, of the same or of different types and result in an infinite periodic entangled array; (2) the number of entangled motifs can be finite or infinite; (3) all of the constituent motifs have lower dimensionality than that of resultant architectures; (4) each individual motif is catenated only with the surrounding motifs, but not with all the others, etc. As is the case with MOFs and other coordination polymers, the terms polycatenation and interpenetration are sometimes not rigidly defined as outlined above.

The number of interpenetrated POM-based coordination polymers is limited; according to the classification standards mentioned above, the existing examples of interpenetration are classified into two categories: a single motif in 2D (Section 2.1) and a single motif in 3D (Section 2.2).

2.1. Interpenetration based on 2D layers

The compounds in this category are composed of 2D frameworks and usually have large open voids in a single network. After interpenetrating, these voids are filled and a 2D → 2D interpenetrating framework is formed. The *n*-fold 2D nets may stack directly on top of each other, generating a 3D supermolecular crystal packing structure, but strictly speaking, they are still 2D frameworks. As for the example which has an increased dimensionality after interpenetrating, just like the 2D + 2D → 3D framework, this will be described in detail when discussing polycatenation.

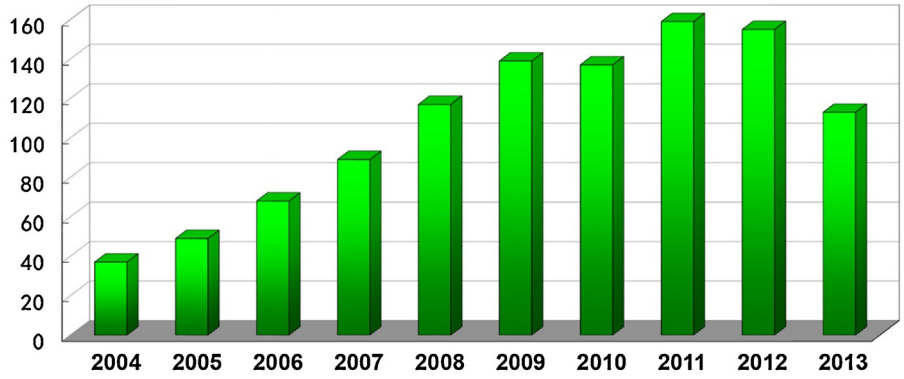

Scheme 1. The increasing number of articles dealing with POM-based coordination polymers encompassed by the Web of Knowledge (1119 in total) until September 2013.

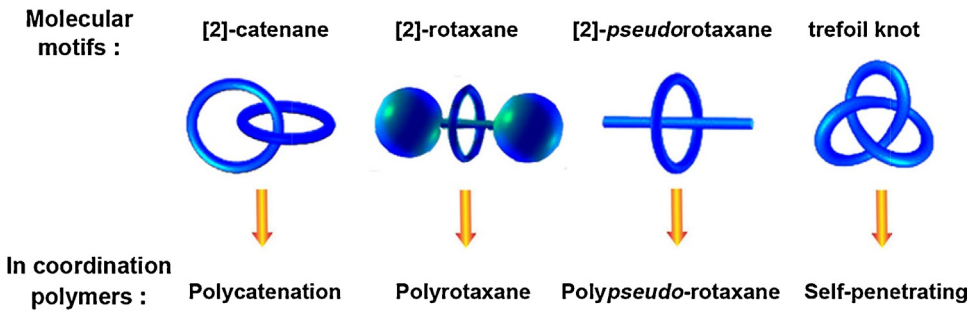

Scheme 2. Mechanical bonds from the molecular motifs to the coordination polymers.

A typical example of this type (2D → 2D) was reported by Lu and co-workers in 2010. Compound $[(Ag_4(4,4'\text{-}H_2bpz)_4)(SiW_{12}O_{40})]$ (**1**) (The corresponding formulae and the ligand abbreviations of related compounds are listed in Table 1) was obtained at 180 °C by a hydrothermal reaction [30]. In this structure, two kinds of silver atom coordinate with N atoms from 4,4′-H_2bpz ligands to form castellated $[Ag(4,4'\text{-}H_2bpz)]_n$ chains, which connect two neighboring castellated chains by μ_2-$[SiW_{12}O_{40}]^{4-}$ polyoxometalate anions to form a unique 2D framework with large rhombic cavities. The resulting sheets are identical and stack in an ABC fashion. The large cavities in the sheets are occupied by polyanions, forming a densely packed 2D parallel 3-fold interpenetration architecture (Fig. 1).

In addition, the complexes $[Cu^I{}_4(ttb)_3(\beta\text{-}Mo_8O_{26})]$ (**2**) [31] and $[M_2(L1)_3(H_2O)_4][\beta\text{-}Mo_8O_{26}]\cdot 2H_2O$ (M = Zn (**3**), Co (**4**), and Ni (**5**)) [32] also display similar 2D interpenetrating structures. In all these compounds, POMs act as linkers in the individual motifs except for compound **2**, in which β-$[Mo_8O_{26}]^{4-}$ anions with the monodentate coordination modes just hang in the tubular channels of the 2D layer (Schemes 4 and 5).

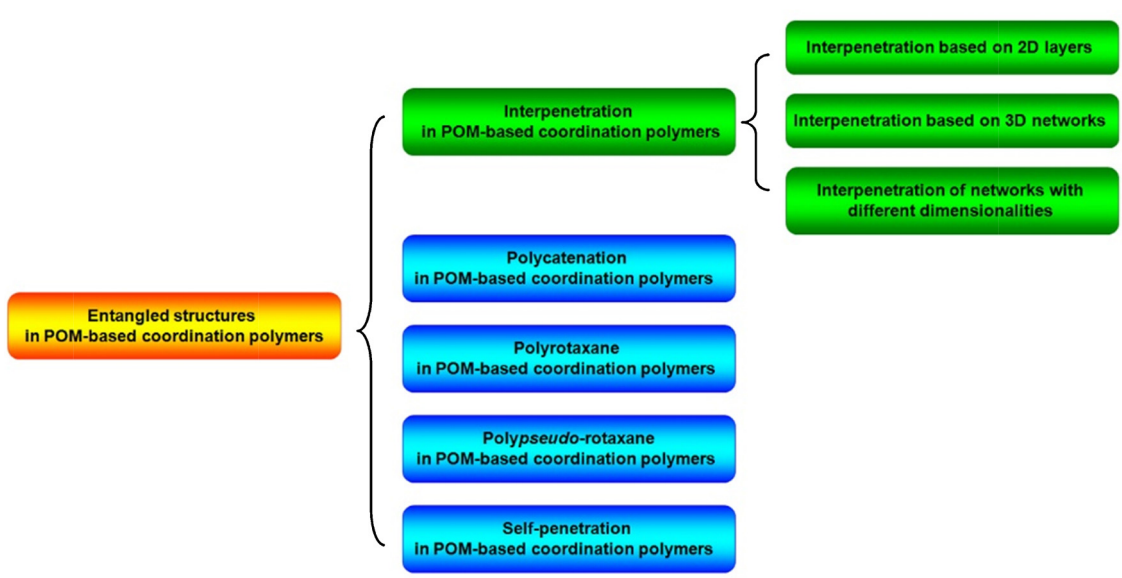

Scheme 3. Classification of POM-based coordination polymers with entangled structure.

Table 1
Selected structural information for POM-based coordination polymer.[a]

No	Compound	CCDC refcode	POM	Motif dimension	RCSR name of the motif	Final dimension	Degree	The role of POM	Topology	Ref
1	$[(Ag_4(4,4'\text{-}H_2bpz)_4)(SiW_{12}O_{40})]$	716731	$[SiW_{12}O_{40}]^{4-}$	2D	hcb	2D	3-fold	Linker	2D layer Interpenetration	[30]
2	$[Cu^{I}_4(ttb)_3(\beta\text{-}Mo_8O_{26})]$	789620	$\beta\text{-}[Mo_8O_{26}]^{4-}$	2D	N[b]	2D	2-fold	Pendant	2D layer Interpenetration	[31]
3, 4, 5	$[M_2(L1)_3(H_2O)_4][\beta\text{-}Mo_8O_{26}]\cdot 2H_2O$, M = Zn (**3**), Co (**4**), and Ni (**5**)	692093 692084 692085	$\beta\text{-}[Mo_8O_{26}]^{4-}$	2D	hcb (Zn), hcb (Co), hcb (Ni)	2D	2-fold	Linker	2D layer Interpenetration	[32]
6	$[Cu^{II}(bbi)_2(H_2O)(\beta\text{-}Mo_8O_{26})_{0.5}]$	707001	$\beta\text{-}[Mo_8O_{26}]^{4-}$	3D	fsc	3D	2-fold	Linker	3D framework Interpenetration	[33]
7	$[Ni(BIMB)_2(\gamma\text{-}Mo_8O_{26})_{0.5}]\cdot 3H_2O$	777261	$\gamma\text{-}[Mo_8O_{26}]^{4-}$	3D	mog	3D	2-fold	Linker	3D framework Interpenetration	[34]
8, 9	$[Cu_6(L1)_6(HPM_{12}O_{40})]\cdot 2H_2O$, M = Mo (**8**), W (**9**)	694259 694260	$[HPMo^{VI}_8Mo^{V}_4O_{40}]^{6-}$ (**8**) $[HPW^{VI}_8W^{V}_4O_{40}]^{6-}$ (**9**)	3D	N	3D	2-fold	Linker	3D framework Interpenetration	[35]
10	$[Cu(bbi)]_5H[H_2W_{12}O_{40}]$	710054	$\alpha\text{-}H[H_2W_{12}O_{40}]^{5-}$	3D	nor	3D	2-fold	Linker	3D framework Interpenetration	[36]
11	$Li_3[(Rh_2(CH_3COO)_4)_2(PW_{12}O_{40})]\cdot 12.5H_2O$	872093	$[PW_{12}O_{40}]^{3-}$	3D	pcu	3D	2-fold	Linker	3D framework Interpenetration	[37]
12	$[Co_2(H_2O)_2(btb)_4(HPMo^{VI}_{10}Mo^{V}_2O_{40})]$	853727	$[PMo^{VI}_{10}Mo^{V}_2O_{40}]^{5-}$	3D	N	3D	2-fold	Linker	3D framework Interpenetration	[38]
13	$[Cu^{II}_2(ttb)_2(\beta\text{-}Mo_8O_{26})(H_2O)_2]\cdot 2H_2O$	789618	$\beta\text{-}[Mo_8O_{26}]^{4-}$	3D	N	3D	2-fold	Linker	3D framework Interpenetration	[31]
14	$Cu^{I}_4(ttb)_2(\beta\text{-}Mo_8O_{26})(H_2O)$	789619	$\beta\text{-}[Mo_8O_{26}]^{4-}$	3D	N	3D	2-fold	Linker	3D framework Interpenetration	[31]
15	$[Cd_2(H_2O)_2(btb)_4(SiMo_{12}O_{40})]$	783860	$[SiMo_{12}O_{40}]^{4-}$	3D	nov	3D	2-fold	Linker	3D framework Interpenetration	[39]
16	$[Ag_2(4,4'\text{-bpy})_2(4,4'\text{-Hbpy})(H_2O)][PW_{12}O_{40}]$	733468	$[PW_{12}O_{40}]^{3-}$	3D	dia	3D	3-fold	Linker	3D framework Interpenetration	[40]
17	$[Cu_2(4,4'\text{-bpy})_2(Hbpy)(H_2O)](PW_{12}O_{40})$	701152	$[PW_{12}O_{40}]^{3-}$	3D	dia	3D	3-fold	Linker	3D framework Interpenetration	[41]
18	$[Cu^{I}_5(4,4'\text{-bpy})_5(H_2O)_2][[Cu^{II}(H_2O)_3]_2Cu^{II}[P_4Mo^{V}_6O_{25}(OH)_6]_2]\cdot H_3O^{+}\cdot 2H_2O$	631162	$[P_4Mo_6O_{31}]^{12-}$	3D	N	3D	4-fold	Linker	3D framework Interpenetration	[42]
19	$[(4,4'\text{-bpy})_7Cu^{I}_7Cl_2(BW_{12}O_{40})]\cdot H_2O$	671760	$[BW_{12}O_{40}]^{5-}$	3D	tfc	3D	5-fold	Linker	3D framework Interpenetration	[43]
20	$[(4,4'\text{-bpy})_7Cu^{I}_7Cl_2(PW^{VI}_{10}W^{V}_2O_{40})]\cdot 1.5H_2O$	607895	$[PW^{VI}_{10}W^{V}_2O_{40}]^{5-}$	3D	tfc	3D	5-fold	Linker	3D framework Interpenetration	[44]
21	$[Cu_3(4,4'\text{-bpy})_5]_2[H_2SiW_{11}O_{39}]\cdot 5H_2O$	736061	$[SiW_{11}O_{39}]^{8-}$	3D	N	3D	4-fold	Template	3D framework Interpenetration	[45]
22	$[Ag_3(tptz)_3][(Mo_5O_{17})](H_3O)(H_2O)_{1.5}$	857703	$[Mo_5O_{17}]^{4-}$	3D	ths	3D	3-fold	Template	3D framework Interpenetration	[46]
23	$[Ni_3(btb)_5][PMo_{12}O_{40}]_2\cdot 14H_2O$	798687	$[PMo_{12}O_{40}]^{3-}$	3D	mog	3D	2-fold	Linker and template	3D framework Interpenetration	[47]
24	$Ag_7(bbi)_5(OH)(P_2W_{18}O_{62})$	775926	$\alpha\text{-}[P_2W_{18}O_{62}]^{6-}$	3D + 2D		3D		Linker	2D + 3D interpenetrating framework	[48]
25	$Cu^{II}Cu^{I}_2(L1)_5[\beta\text{-}Mo_8O_{26}]$	832447	$\beta\text{-}[Mo_8O_{26}]^{4-}$	3D + 2D		3D		Linker	2D + 3D interpenetrating framework	[49]
26	$\{[Ag_2(trz)_2][Ag_{24}(trz)_{18}]\}[PW_{12}O_{40}]_2$	745116	$[PW_{12}O_{40}]^{3-}$	0D		3D		Template	(0D→3D) polycatenated framework	[50]
27	$\{Cu_3(4,4'\text{-bpy})_3(H_2O)[PMo_{12}O_{40}(VO)_2]\cdot 5H_2O\}_n$	271165	$[PMo^{VI}_8Mo^{V}_4O_{40}(V^{IV}O)_2]^{3-}$	1D		3D		Linker	(1D→3D) polycatenated framework	[51]
28	$[Cu^{II}(btp)_2(H_2O)][\beta\text{-}Mo_8O_{26}]_{0.5}\cdot 2H_2O$	757940	$\beta\text{-}[Mo_8O_{26}]^{4-}$	2D		3D		Linker	(2D→3D) polycatenated framework	[52]
29	$[Cu^{II}(btp)_2(H_2O)(\beta\text{-}Mo_8O_{26})_{0.5}]\cdot H_2O$	787907	$\beta\text{-}[Mo_8O_{26}]^{4-}$	2D		3D		Linker	(2D→3D) polycatenated framework	[53]
30	$[Ag_6(Tipa)_4(\beta\text{-}Mo_8O_{26})][H_2(\beta\text{-}Mo_8O_{26})]\cdot 5H_2O$	844767	$\beta\text{-}[Mo_8O_{26}]^{4-}$	2D		3D		Linker	(2D→3D) polycatenated framework	[54]

Table 1 (*Continued*)

No	Compound	CCDC refcode	POM	Motif dimension	RCSR name of the motif	Final dimension	Degree	The role of POM	Topology	Ref
31	$[Cu^{I}_4(L3)_4Mo_6O_{18}(O_3AsPh)_2]$	928455	$[Mo_6O_{18}(O_3AsPh)_2]^{4-}$	2D		3D		Linker	(2D→3D) polycatenated framework	[55]
32	$[Cu_2(bpp)_4(H_2O)_2](SiW_{12}O_{40})\sim 6H_2O$	642469	$[SiW_{12}O_{40}]^{4-}$	2D		3D		Template	(2D→3D) polycatenated framework	[56]
33	$[Cu_2(L4)_3(H_2O)_6][SiMo_{12}O_{40}]\cdot 9H_2O$	850464	$[SiMo_{12}O_{40}]^{4-}$	1D		2D		Template	(1D→2D) polyrotaxane	[57]
34	$[Cu_2(L4)_3(H_2O)_6][SiW_{12}O_{40}]\cdot 6H_2O$	850465	$[SiW_{12}O_{40}]^{4-}$	1D		2D		Template	(1D→2D) polyrotaxane	[57]
35	$[Cu^{I}_3(L5)_2(Mo_8O_{26})_{0.5}Cl]$	727454	$[Mo_8O_{26}]^{4-}$	2D		2D		Linker	(2D→2D) polyrotaxane	[58]
36	$[Cu^{II}(L6)_2(H_2O)_2][Cu^{I}_2(L6)_2]PMo_{12}O_{40}$	298626	$[PMo^{V}Mo^{VI}_{11}O_{40}]^{4-}$	3D + 0D		3D		Template	3D + 3D + 0D 2-fold interpenetrated structure by the unusual rotaxane mode	[59]
37	$[Cu^{II}(bbi)_2(\alpha\text{-}Mo_8O_{26})][Cu^{I}(bbi)]_2$	707002	α-$[Mo_8O_{26}]^{4-}$	3D + 1D		3D		Linker	3D + 1D polypseudo-rotaxane architecture	[33]
38	$[Cu^{II}Cu^{I}(bbi)_3(\alpha\text{-}Mo_8O_{26})][Cu^{I}(bbi)]$	707003	α-$[Mo_8O_{26}]^{4-}$	3D + 1D		3D		Linker	3D + 1D polypseudo-rotaxane architecture	[33]
39	$[Cu^{I}(bix)][(Cu^{I}bix)\ (\delta\text{-}Mo_8O_{26})_{0.5}]$	723237	δ-$[Mo_8O_{26}]^{4-}$	3D + 1D		3D		Linker	3D + 1D polypseudo-rotaxane architecture	[60]
40	$H(Cu^{I}bix)[(Cu^{I}bix)_2(\beta\text{-}Mo_8O_{26})]\cdot 2H_2O$	723238	β-$[Mo_8O_{26}]^{4-}$	3D + 1D		3D		Linker	3D + 1D polypseudo-rotaxane architecture	[60]
41, 42	$[M_4(bix)_4][\delta\text{-}Mo_8O_{26}]$, M = Cu (41), Ag (42)	692090 692091	δ-$[Mo_8O_{26}]^{4-}$	3D + 1D		3D		Linker	3D + 1D polypseudo-rotaxane architecture	[32]
43	$[Cu(bbi)_2V_{10}O_{26}][Cu(bbi)]_2\cdot H_2O$	658057	$[V_{10}O_{26}]^{4-}$	3D + 1D		3D		Linker	3D + 1D polypseudo-rotaxane architecture	[61]
44	$[Cd(BPE)(\alpha\text{-}Mo8O26)][Cd(BPE)(DMF)_4]\cdot 2DMF$	272193	α-$[Mo_8O_{26}]^{4-}$	2D + 1D		3D		Linker	2D + 1D polypseudo-rotaxane architecture	[62]
45	$[Cu^{I}_2(cis\text{-}btp)_2][Cu^{I}_2(trans\text{-}btp)_2Mo_6O_{18}(O_3AsPh)_2]$	928453	$[Mo_6O_{18}(O_3AsPh)_2]^{4-}$	2D + 1D		3D		linker	2D + 1D polypseudo-rotaxane architecture	[55]
46	$[Cu(bbi)]_2[Cu_2(bbi)_2(\delta\text{-}Mo_8O_{26})_{0.5}][\alpha\text{-}Mo_8O_{26}]_{0.5}$	681862	δ-$[Mo_8O_{26}]^{4-}$ α-$[Mo_8O_{26}]^{4-}$	2D + 1D		3D		Linker	2D + 1D polypseudo-rotaxane architecture	[63]
47	$[Cu(bbi)][Cu(bbi)(\theta\text{-}Mo_8O_{26})_{0.5}]$	681863	θ-$[Mo_8O_{26}]^{4-}$	2D + 1D		3D		Linker	2D + 1D polypseudo-rotaxane architecture	[63]
48	$[Na_2(H_2O)_8Ag_2(HINA)_3(INA)][Na(H_2O)_2Ag_2(HINA)_4(H_2W_{12}O_{40})]\cdot 2H_2O$	689266	$[H_2W_{12}O_{40}]^{6-}$	2D + 1D		3D		Linker	2D + 1D polypseudo-rotaxane architecture	[64]
49	$[Cu(L1)]_4[SiMo_{12}O_{40}]$	703663	$[SiMo_{12}O_{40}]^{4-}$	2D + 1D		3D		Linker	2D + 1D polypseudo-rotaxane architecture	[65]
50	$[Cu(L6)_2(HPW^{VI}_{10}W^{V}_2O_{40})][Cu(L6)(H_2O)_4]\cdot 4H_2O$	831765	$[PW_{12}O_{40}]^{3-}$	2D + 1D		3D		Linker	2D + 1D polypseudo-rotaxane architecture	[66]
51	$[Ag_5(L7)_5][K_2(OH)P_2W_{18}O_{62}]\cdot H_2O$	885334	$[P_2W_{18}O_{62}]^{6-}$	2D + 1D		3D		Linker (chain)	2D + 1D polypseudo-rotaxane architecture	[67]
52	$[Cu_4(L1)_4][\beta\text{-}Mo_8O_{26}]_{0.5}[\gamma\text{-}Mo_8O_{26}]_{0.5}\cdot H_2O$	692088	β-$[Mo_8O_{26}]^{4-}$ γ-$[Mo_8O_{26}]^{4-}$	1D + 1D		3D		Linker	1D + 1D polypseudo-rotaxane architecture	[32]

Table 1 (*Continued*)

No	Compound	CCDC refcode	POM	Motif dimension	RCSR name of the motif	Final dimension	Degree	The role of POM	Topology	Ref
53	$[Ag_{0.52}Na_{0.48}(\beta\text{-}Mo_8O_{26})(H_2O)][Ag_3(Tipa)_2]$	844766	$\beta\text{-}[Mo_8O_{26}]^{4-}$	1D + 1D		3D		Linker (chain)	1D + 1D polypseudo-rotaxane architecture	[54]
54	$(bix)[Cu(bix)][Cu_2(bix)_2(P_2W_{18}O_{62})]\cdot 2H_2O$	723254	$[P_2W_{18}O_{62}]^{6-}$	1D + 1D		3D		Linker	1D + 1D polypseudo-rotaxane architecture	[68]
55	$[Ag(L1)]_4[SiMo_{12}O_{40}]\cdot 2H_2O$	703662	$[SiMo_{12}O_{40}]^{4-}$	0D + 1D		2D		Template	0D + 1D polypseudo-rotaxane architecture	[65]
56	$[Cu(L8)]_2(HPW_{12}O_{40})\cdot 3H_2O$	821332	$[PW_{12}O_{40}]^{3-}$	0D + 1D		3D		Template	0D + 1D polypseudo-rotaxane architecture	[69]
57	$[(AgL7)_2\text{-}Ag_2(L7)_2][(SiW_{12}O_{40})]$	885332	$[SiW_{12}O_{40}]^{4-}$	0D + 1D		3D		Template	0D + 1D polypseudo-rotaxane architecture	[67]
58	$[Cu^{I}{}_3(L1)_3][\{Cu^{II}(L1)_2\}\{PMo_{12}O_{40}(VO)_2\}]\cdot H_2O$	626881	$[PMo^{V}{}_6Mo^{VI}{}_6O_{40}(V^{IV}O)_2]^{5-}$	3D + 2D		3D		Linker	Both polyrotaxane and polycatenane characters	[70]
59, 60, 61	$[M_2(H_2O)_4(L1)_3][SiMo_{12}O_{40}]\cdot 4H_2O$, M= Mn (59), Ni (60) and Co (61)	703666 703667 703668	$[SiMo_{12}O_{40}]^{4-}$	2D		2D		Linker	Both polyrotaxane and polycatenane characters	[65]
62	$Ag_{14}(trz)_{10}[SiW_{12}O_{40}]$	789149	$[SiW_{12}O_{40}]^{4-}$	1D		3D		Template	Both polyrotaxane and polycatenane characters	[71]
63	$[Ni_2(bbi)_2(H_2O)_4V_4O_{12}]\cdot 2H_2O$	683857	$(VO_3)^-$ $(V_2O_6)^{2-}$		N	3D		Linker	Self-penetrating network	[72]
64	$[Cu_5(btx)_4(PMo^{VI}{}_{10}Mo^{V}{}_2O_{40})]$	682175	$[PMo^{VI}{}_{10}Mo^{V}{}_2O_{40}]^{5-}$		3,3,4,6T14 (MOF.ttd)	3D		Linker	Self-penetrating network	[73]
65	$[Cu^{I}{}_5(btx)_4(PW^{VI}{}_{10}W^{V}{}_2O_{40})]$	860727	$[PW^{VI}{}_{10}W^{V}{}_2O_{40}]^{5-}$		3,3,4,6T14 (MOF.ttd)	3D		Linker	Self-penetrating network	[74]
66	$[Cu^{I}{}_{12}(bmtr)_9(HSiMo_{12}O_{40})_4]$	832844	$[SiMo_{12}O_{40}]^{4-}$		N	3D		Linker	Self-penetrating network	[75]
67	$[Ag_6Cl_2(mmt)_4(H_4SiMo_{12}O_{40})(H_2O)_2]$	852618	$[SiMo_{12}O_{40}]^{4-}$		N	3D		Linker	Self-penetrating network	[76]
68	$[Cu_3(btx)_{5.5}(P_2W_{18}O_{62})]\cdot 4H_2O$	664328	$[P_2W_{18}O_{62}]^{6-}$		4,5,5,6T6 (MOF.ttd)	3D		Linker	Self-penetrating network	[77]
69	$[Co_2(btb)_4(H_2O)][H_2P_2W_{18}O_{62}]\cdot 3H_2O$	885574	$[P_2W_{18}O_{62}]^{6-}$		N	3D		Linker	Self-penetrating network	[78]
70	$[Co_2(btb)_4(H_2O)][H_2As_2W_{18}O_{62}]\cdot 6H_2O$	885575	$[As_2W_{18}O_{62}]^{6-}$		N	3D		Linker	Self-penetrating network	[78]
71	$[Ni_2(BIMB)_2(Mo^{VI}{}_4Mo^{V}{}_2O_{19})]$	778999	$[Mo^{VI}{}_4Mo^{V}{}_2O_{19}]^{4-}$		N	3D		Linker	Self-penetrating network	[79]
72	$[(4,4'\text{-bpy})_6Cu^{I}{}_6Cl_3(Mo^{V}W_5O_{19})]$	671761	$[Mo^{V}W_5O_{19}]^{3-}$		ilc	3D		Linker	Self-penetrating network	[43]
73	$[Cu^{I}{}_4(btb)_4Mo_6O_{18}(O_3AsPh)_2]$	928454	$[Mo_6O_{18}(O_3AsPh)_2]^{4-}$		N	3D		Linker	Self-penetrating network	[55]
74	$[Zn(BIMB)_2(\gamma\text{-}Mo_8O_{26})_{0.5}]$	777262	$[Mo_8O_{26}]^{4-}$		N	3D		Linker	Self-penetrating network	[34]
75	$[Cu_3(BIMB)_4(H_2O)(\delta\text{-}Mo_8O_{26})Cl_2]\cdot 3H_2O$	777263	$\delta\text{-}[Mo_8O_{26}]^{4-}$		N	3D		Linker	Self-penetrating network	[34]
76	$[Cu^{II}{}_2(btx)_4][\alpha\text{-}Mo_8O_{26}]$	769068	$\alpha\text{-}[Mo_8O_{26}]^{4-}$		N	3D		Linker	Self-penetrating network	[80]
77	$[Ag_2(2,4'\text{-tmbpt})_2(\alpha\text{-}Mo_8O_{26})_{0.5}(H_2O)_{0.5}]\cdot 2H_2O$	912410	$\alpha\text{-}[Mo_8O_{26}]^{4-}$		sql	3D		Linker	Self-penetrating network	[81]
78	$[Ni(btb)_2(H_2O)][\gamma\text{-}Mo_8O_{26}]_{0.5}\cdot H_2O$	793725	$\gamma\text{-}[Mo_8O_{26}]^{4-}$		N	3D		Linker	Self-penetrating network	[82]
79	$Cu^{I}{}_8(L1)_6[(\alpha\text{-}Mo_8O_{26})(\beta\text{-}Mo_8O_{26})]$	832445	$\alpha\text{-}[Mo_8O_{26}]^{4-}$ $\beta\text{-}[Mo_8O_{26}]^{4-}$		N	3D		Linker	Self-penetrating network	[49]

[a] *Abbreviations*: 4,4′-H_2bpz = 3,3′,5,5′-tetramethyl-substituted 4,4′-bipyrazole; ttb = 1,3,5-tris(1,2,4-triazol-1-ylmethyl)-2,4,6-trimethyl benzene; L1 = 1,4-bis(1,2,4-triazol-1-ylmethyl)benzene; bbi = 1,1′-(1,4-butanediyl)bis(imidazole); BIMB = 1,4-bis(1-imidazolyl)benzene; btb = 1,4-bis(1,2,4-triazol-1-yl)butane; 4,4′-bpy = 4,4′-bipyridine; L2 = 1,4-bis(pyridinil-4-carboxylato)-l,4-dimethylbenzene; tptz = 2,4,6-tri(4-pyridyl)-1,3,5-triazine; trz = 1,2,4-triazole; btp = 1,3-bis(1,2,4-triazol-1-yl)propane; Tipa = tri(4-imidazolylphenyl)amine; L3 = 1,5-bis(1,2,4-triazol-1-yl)pentane; bpp = 1,3-bis(4-pyridyl)propane; L4 = N,N′-bis(3-pyridinecarboxamide)-1,4-butane; L5 = 3-((1H-1,2,4-triazol-1-yl)methyl)pyridine; L6 = 4,4′-bis(1,2,4-triazol-1-ylmethyl)biphenyl; bix = 1,4-bis(imidazole-1-ylmethyl)benzene; BPE = 1,2-bis(4-pyridyl)ethane; HINA = isonicotinic acid; L7 = 1,3-bis(imidazol-1-ylmethyl)benzene; L8 = 1,4-bis(imidazol-1-ylmethyl)biphenyl; btx = 1,6-bis(1,2,4-triazol-1-y1)hexane; bmtr = 1,3-bis(1-methyl-5-mercapto-1,2,3,4-tetrazole)propane; mmt = 1-methyl-5-mercapto-1,2,3,4-tetrazole; 2,4′-tmbpt = 1-((1H-1,2,4-triazol-1-yl)methyl)-3-(4-pyridyl)-5-(2-pyridyl)-1,2,4-triazole).

[b] N: Topological name of this compound is not given in RCSR.

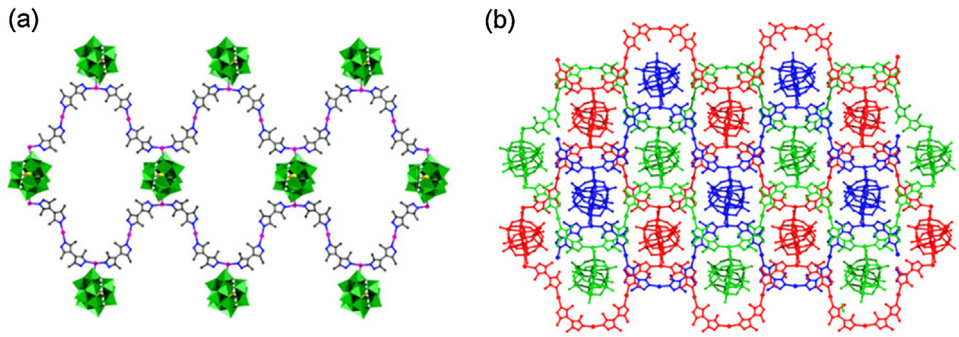

Fig. 1. (a) Structural view of compound **1** showing its 2D sheet constructed from 1D castellated chains and Keggin anions with large pores. (b) A view of the 3-fold interpenetration sheet of compound **1**.

2.2. Interpenetration based on 3D networks

Generally, interpenetration in 3D structures is more common when compared with POM-based coordination polymers with lower dimensionalities. As discussed earlier, the presence of an individual net with sufficiently large void space is a basic element of an interpenetration framework. Such motifs have been found in a number of 3D to 3D POM-based coordination polymers. The degree of interpenetration will also be discussed in detail here. Examples of existing 3D networks can be classified into three species according to the role of the POMs in the whole framework: POMs act as linkers to generate each single motif (Section 2.2.1), POMs act as templates existing in the channels (Section 2.2.2) and POMs act as linkers and templates (Section 2.2.3).

2.2.1. POMs act as linkers to generate each single motif

In 2008, Lan et al. successfully isolated the 2-fold interpenetrating complex $[Cu^{II}(bbi)_2(H_2O)(\beta\text{-}Mo_8O_{26})_{0.5}]$ (**6**) [33] through combination of the bbi ligand, $(NH_4)_6Mo_7O_{24}\cdot 4H_2O$ and $Cu(NO_3)_2\cdot 3H_2O$ at pH ≈ 3. In this species, two kinds of bbi ligand coordinate to Cu^{II} cations to generate a 2D (4, 4) sheet. β-$[Mo_8O_{26}]^{4-}$ coordinates to two Cu^{II} cations with two terminal oxygen atoms to form an intricate 3D framework. The void space in a single framework is so large that two identical 3D frameworks interpenetrate each other to form a unique 2-fold interpenetration of the architecture (Fig. 2a). Based on different POMs, ligands and metals, 3D interpenetration frameworks (**7**–**20**) with different degrees of interpenetration, ranging from 2-fold to 5-fold, have been constructed (details of these compounds are shown in Table 1).

2.2.2. POMs act as templates existing in the channels

In 2010, Yang and co-workers successfully isolated block crystals of $[Cu_3(4,4'\text{-bpy})_5]_2[H_2SiW_{11}O_{39}]\cdot 5H_2O$ (**21**) by a hydrothermal method [45]. In **21**, each Cu center is connected to another via 4,4′-bpy ligands resulting in a 3D Cu–organic framework. Considering Cu as nodes and 4,4′-bpy as linkers, the structure of **21** is a single 3D (3,4)-connected network. Two generating 3D nets present a 2-fold interpenetrating structure, which is extended to the whole 3D 4-fold interpenetrating structure via translation movement. Topological analysis of the interpenetration reveals that two identical interpenetrating nets can be exactly overlapped only by translation and the translating vector is 28.35 Å along the *b*-axis. Even with this interpenetration, the overall 3D nets still possess a significant void space that can accommodate nanosized polyoxoanions $[SiW_{11}O_{39}]^{8-}$ (~10.3 Å in diameter) as guests (Fig. 3).

The complex $[Ag_3(tptz)_3(Mo_5O_{17})](H_3O)(H_2O)_{1.5}$ (**22**) [46] accommodates POMs as guests and the degree of interpenetration of this compound is 3-fold. Topological analysis of **22** reveals that, considering Ag(I) ions and the tptz ligands as 3-connected nodes, each single Ag-organic framework can be simplified as a 3-connected net with 10^3 topology.

2.2.3. POMs act as linkers and templates

In 2011, Wang et al. described an interesting 3D POM-based complex $[Ni_3(btb)_5][PMo_{12}O_{40}]_2\cdot 14H_2O$ (**23**) containing two

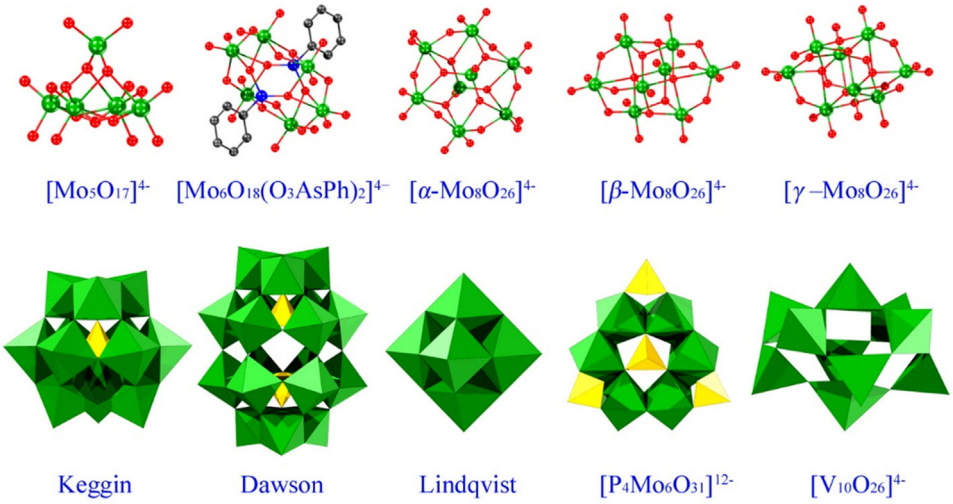

Scheme 4. The POM units mentioned in this review.

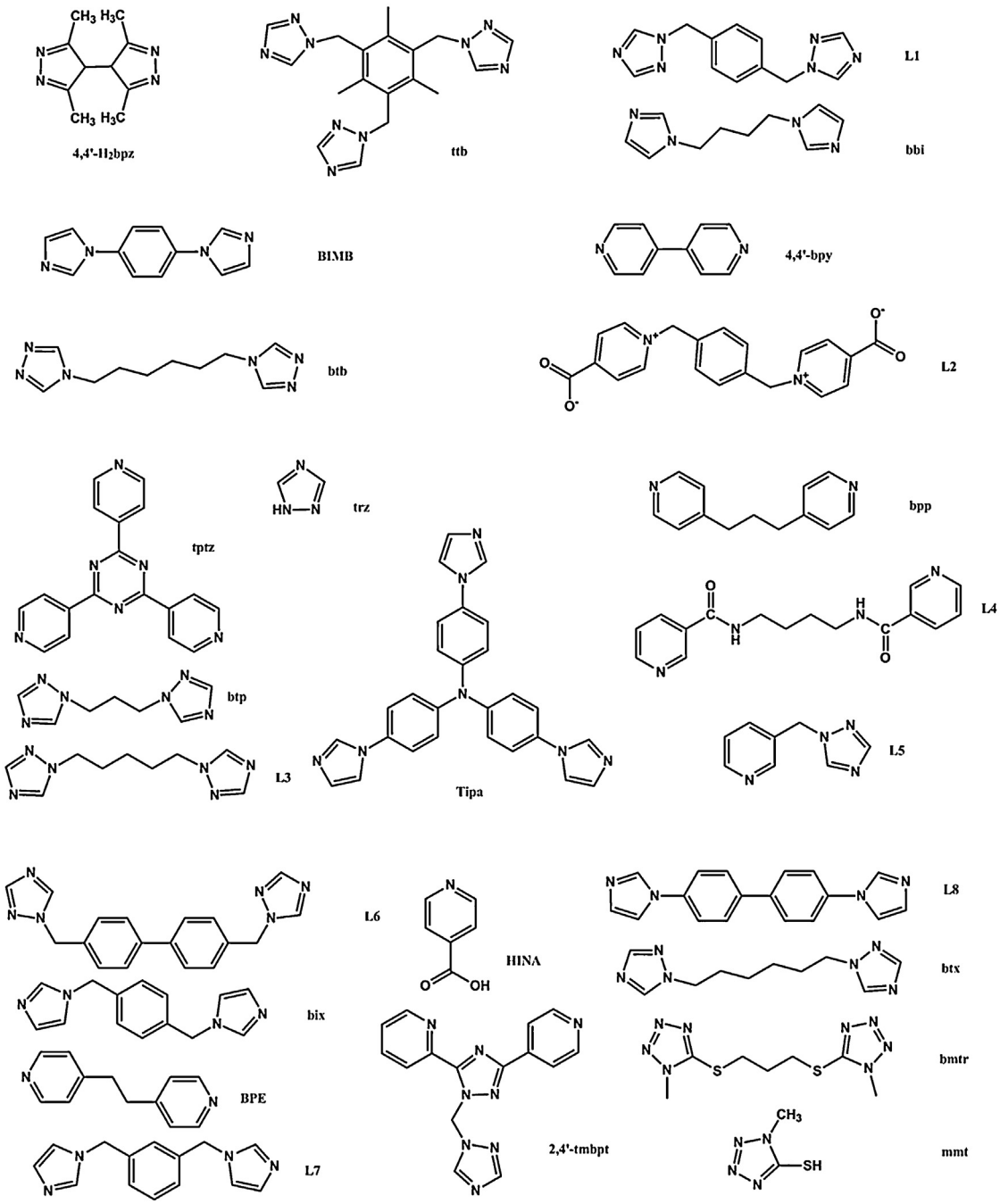

Scheme 5. The ligands mentioned in this review.

different kinds of $[PMo_{12}O_{40}]^{3-}$ anions [47]. A notable feature in the structure of compound **23** is that the Ni1, Ni2 ions and three types of btb ligands form an interesting 2D net with two different kinds of grid-like chains which share two Ni ions. One kind of $[PMo_{12}O_{40}]^{3-}$ anion, offering two terminal O atoms, acts as a two-connected ligand to link two 2D nets via Ni1 ions. Thus, a 3D MOF is formed, in which Keggin anions exert their linkage roles. Furthermore, two sets of these 3D MOFs interpenetrate with each other to form a 2-fold interpenetrating structure, which has two different channel sizes. Another kind of $[PMo_{12}O_{40}]^{3-}$ anion acting as an inorganic template is only incorporated into the bigger hexagonal channels. In this case, the POMs act not only as the linkers to generate each single motif but also the templates existing in the channels.

2.3. Interpenetration of networks with different dimensionalities

Like other non-POM-based coordination polymers, the interpenetration between identical networks, termed homo-interpenetrating nets, is quite common because the identical molecular fragments favor the same periodicity. In contrast, the interpenetration between different structures, termed hetero-interpenetrating nets, is relatively rare, especially those with different dimensionalities. Two POM-based compounds belong in this category, in both, POMs act as linkers to form 3D frameworks.

In 2011, an interpenetrated compound based on the Wells–Dawson polyoxometalate, $Ag_7(bbi)_5(OH)(P_2W_{18}O_{62})$ (**24**), was hydrothermally synthesized [48a] by Peng and co-workers. In this 3D framework motif, the α-$[P_2W_{18}O_{62}]^{6-}$ polyanions are

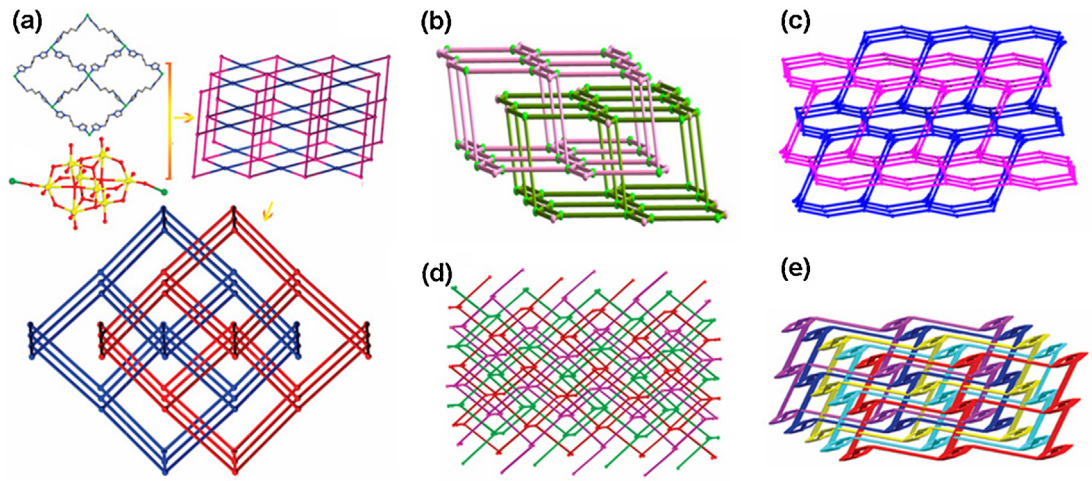

Fig. 2. (a) Schematic view of the 3D (4,6)-connected framework with the $(4^4{\cdot}6^2)(4^4{\cdot}6^{10}{\cdot}8)$ topology in compound **6** (blue and pink balls represent the 4 and 6-connected nodes, respectively) and schematic view of the 2-fold interpenetrating structure of compound **6**. (b) Schematic representation of the 2-fold interpenetration 4-connected 3D framework with the $(4{\cdot}6^4{\cdot}8)_2(4^2{\cdot}6^2{\cdot}8^2)$ topology in compound **7**. (c) Schematic view of the 2-fold interpenetrating 3D (3,4)-connected framework with the $(6^2{\cdot}8^1)_2(6^2{\cdot}8^4)$ topology in compound **14**. (d) Interlocked units of 3-fold interpenetration diamond-like nets of compound **16**. (e) Schematic view of the 5-fold parallel interpenetrating 3D network with the $(6{\cdot}10^2)_2(6{\cdot}10^2)$ topology in compound **20**.

Reproduced from Refs. [33,34,40,44] with permission from ACS© 2007, 2008, 2010 and Elsevier© 2011.

linked by the supported $\{Ag_2\}^{2+}$ dimers through W—O—Ag bonds to form one-dimensional (1D) $\{Ag_2\}^{2+}$-P_2W_{18} chains, which are further extended to a 2D layer (layer $\{Ag_2\}^{2+}$-P_2W_{18}-Ag4) via horizontal connections of Ag4–bbi segments. The 2D layers are then connected to a 3D framework by the longitudinal extension of Ag5–bbi segments. In the 2D layer motif, bbi and Ag^+ bond together to form a meso-helix chain. These chains are subsequently stitched into a 2D layer with loops by the unsupported Ag7···Ag7 dimers. The huge loop is alternately threaded by the staff of $\{Ag_2\}^{2+}$-P_2W_{18} and Ag4–bbi from three grid layers of $\{Ag_2\}^{2+}$-P_2W_{18}-Ag4. As a result, a 2D + 3D interpenetrating framework is formed (Fig. 4a).

Compound **24** represents the first Wells–Dawson POM-based interpenetrating framework. The short $Ag^I\cdots Ag^I$ interactions existing in the formation of this interpenetrating architecture are crucial. Ag^I is a prominent metal linker in POM-based coordination polymers not only for its abundant coordination modes, but also for its potential applications. Careful solvent and ligand control can be conducive to $Ag^I\cdots Ag^I$ interactions and favor the formation of $\{Ag_2\}^{2+}$ dimers. These self-organizing $\{Ag_2\}^{2+}$ dimers are stabilized by argentophilic metal–metal interactions and usually act as linking units in conjunction with larger isopolyoxometalates to construct 3D frameworks [48b,c]. In compound **24** the $Ag^I\cdots Ag^I$ interactions play different roles: The supported $\{Ag_2\}^{2+}$ dimers (Ag1···Ag9 and Ag2···Ag2) assist in constructing the 3D motif, but the 3D structure would still be integrated without the $Ag^I\cdots Ag^I$ interactions, whereas the unsupported $\{Ag_2\}^{2+}$ dimers (Ag7···Ag7) play a key role in the formation of the interpenetrating framework, stitching the Ag-bbi chains to the 2D motif to create the interpenetrating structure.

Over the past few years, dozens of POM-based compounds based on $Ag^I\cdots Ag^I$ interactions have been reported. Cronin's group has developed a comprehensive library of POM-based networks incorporating electrophilic Ag(I) as a linking species, and exploited this characteristic to expand possible networks, including the excellent work based on the fusion of $\{Ag_3\}$ and $\{Ag_1\}$ units with $[H_2V_{10}O_{28}]^{4-}$ ($\{V_{10}\}$) clusters [48d] and $\{Ag_2\}^{2+}$ dimers with $[H_4W^{VI}{}_{19}O_{62}]^{6-}$ ($\{W_{19}\}$) clusters [48e]. As opposed to Peng's work discussed above, these structures do not contain entangled features, but they do exhibit supramolecular silver polyoxometalate architectures.

The other example is the compound $Cu^{II}Cu^I{}_2(L1)_5[\beta\text{-}Mo_8O_{26}]$ (**25**) [49] reported by Wang and co-workers in 2012. The adjacent β-$[Mo_8O_{26}]^{4-}$ anions are connected together through Cu1 atoms to form a 1D chain. Such 1D chains resulted in a 3D framework through the metal-organic fragments Cu1–L1. From the topological view, compound **25** exhibits a **pcu** topology. Meanwhile, Cu3 centers are

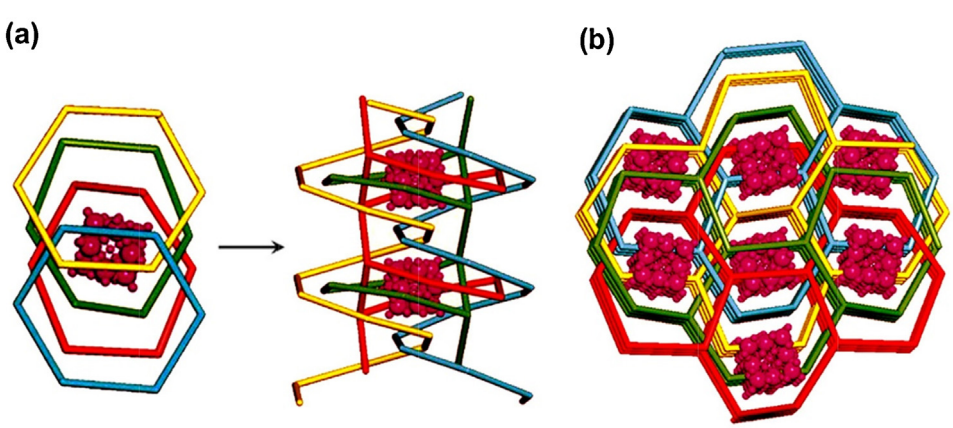

Fig. 3. (a) View of the entangled nanochannel encapsulating Keggin anions. (b) View of the 3D POM-templated 4-fold interpenetrating structure of compound **21**.

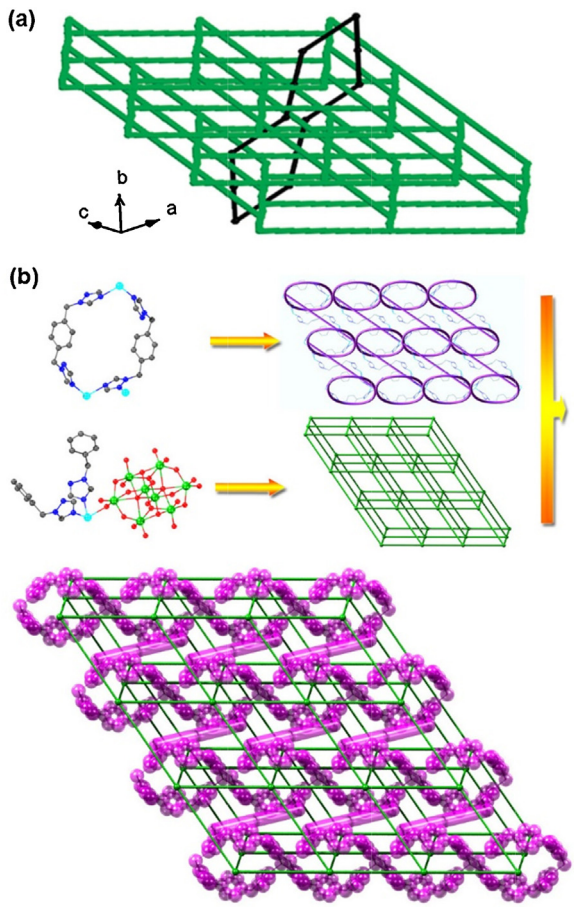

Fig. 4. (a) Interpenetration of the single huge loop and the 3D framework in compound **24**. The huge loop and the 3D framework are shown in black and green, respectively. (b) The representation of 3D interpenetrating polymeric networks formed by 2D poly-ringed structures and **pcu** topology structures interpenetrating each other along the *c* axis in compound **25**.
Reproduced from Ref. [48] with permission from ACS© 2011.

connected together through U-type L1 organic ligands to construct a 1D poly-ringed structure, and adjacent poly-rings are linked together by Cu2 centers and Z-type L1 organic ligands to form 2D poly-ringed layers. The poly-ringed layers and 3D **pcu** topological framework interpenetrate each other along the *c*-axis, leading to a new 2D + 3D interpenetrated polymeric network (Fig. 4b).

In the cases listed above, the long and flexible ligands act as excellent materials for the construction of porous coordination polymer materials; but the destabilizing presence of large free voids in one single network always leads to the formation of interpenetration. The degree of interpenetration reported in the literature thus far generally ranges from 2-fold to 5-fold, with interpenetration above 5-fold being rare in POM-based coordination polymers. The degree of interpenetration may be restricted by the length of the ligands, the size of the POMs and other possible factors. POMs, owing to their various species and strong coordination ability, perform well for motif linkage, as is the case in compounds **6** and **7**. Alternatively, the proper nanoscale size and the high negative charges of the POMs make them perfect anionic templates and charge-compensating guests to stablize the whole framework, as shown in compound **21**. The boundary of one POM acting as a linker or template in the framework is not very well defined. It all depends on the distance between the metal ions in the 2D or 3D skeleton and the oxygen atoms of the POMs. The distance determines the force, and further decides whether one chemical bond between these two particles is considered to be effective or not. According to the common usage in organic chemistry, Walba had suggested that only covalent bonds were topologically significant. In coordination networks, however, a variety of intermolecular forces are at work, including coordinative bonds, hydrogen bonds, metal–oxygen interactions, metal–metal interactions, π-interactions and others. In some situations, whether or not a given chemical force is considered to be effective can drastically change the topology of the individual motifs or even the dimensionality of the whole network. A very good example reflecting this hierarchy of forces is illustrated in compound **37** and compound **38** in Section 4.2.1.

3. Polycatenation in POM-based coordination polymers

To date, polycatenation characters have been described in some POM-based coordination polymers. In the following section, we will list the examples reported in the literatures and will also classify them according to the dimensions of their single motifs (0D, 1D and 2D).

3.1. 0D → 3D polycatenation in POM-based coordination polymers

In 2010, Lu and co-workers reported one vivid example of (0D→3D) polycatenation, $\{[Ag_2(trz)_2][Ag_{24}(trz)_{18}]\}[PW_{12}O_{40}]_2$ (**26**) [50]. It is an excellent example of work in the entanglement study field. Compound **26** exhibits two identical 3D polycatenated architectures, each of which is constructed from mechanical interlocking of 0D adamantane-like molecular cages as building blocks in three directions. The most esthetically pleasing structural feature of compound **26** is its unique polycatenation between discrete octahedral $\{Ag_{24}(trz)_{18}\}^{6+}$ nanocages. Each octahedral nanocage is catenated by six others through all its six vertices. From a topological viewpoint, if each $\{Ag_{24}(trz)_{18}\}^{6+}$ nanocage is considered to be a six-connected node, with the catenation functioning as a linkage between nodes, the structure of compound **26** can be described as a **pcu** topological framework. The void space in a single polycatenated framework is so large that two identical three-dimensional polycatenated frameworks interpenetrate each other to achieve efficient packing. The window-to-window arrangement of the $\{Ag_{24}(trz)_{18}\}^{6+}$ nanocages between the interpenetrating frameworks creates nanosized pores in which $[PW_{12}O_{40}]^{3-}$counteranions are located (Fig. 5).

3.2. 1D → 3D polycatenation in POM-based coordination polymers

In 2006, Peng and co-workers reported one interesting (1D → 3D) polycatenated structure $\{Cu_3(4,4'\text{-bpy})_3(H_2O)[PMo_{12}O_{40}(VO)_2]\cdot 5H_2O\}_n$ (**27**), generated by parallel catenation of molecular ladders [51]. In compound **27**, the Cu atoms are linked together by 4,4′-bpy to form rails of the double ladder, and the polyanion $[PMo^{VI}{}_8Mo^{V}{}_4O_{40}(V^{IV}O)_2]^{3-}$ functions as a rung of the double ladder. Each rectangle of the double ladder is penetrated by two other parallel double ladders that are staggered with each other. Although all the ladders run in the same direction (*b* axis), the staggered interpenetration by the parallel ladders increases the dimensionality of the whole polymeric system and thus leads to the 1D → 3D parallel catenation expansion (Fig. 6a).

3.3. 2D → 3D polycatenation in POM-based coordination polymers

Interlocked 2D layers usually have two distinct classes, parallel and inclined, depending on the relative orientations of the planes of the independent motifs. In the former, all the entangled sheets

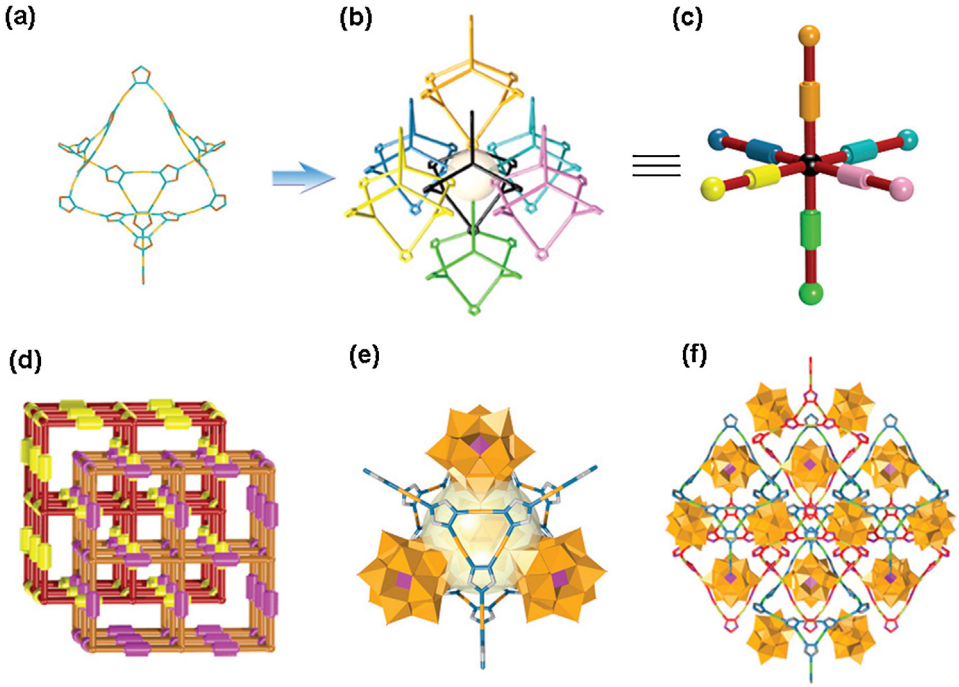

Fig. 5. (a) Discrete $\{Ag_{24}(trz)_{18}\}^{6+}$ nanocages in compound **26**. (b) View of an adamantane-like $\{Ag_{24}(trz)_{18}\}^{6+}$ nanocage catenated by six others through its six vertices to give the (0D → 3D) polycatenation structures. (c) Ball-and-cylinder model representation of (b). Each nanocage is viewed as a six-connected node, with the catenation functioning as linkage between nodes. (d) Schematic view of the 2-fold interpenetrating, infinite extended polycatenated framework. (e) View showing four polyoxometalate species residing in four windows of the adamantane-like nanocage. (f) Structure of $\{[Ag_2(trz)_2][Ag_{24}(trz)_{18}]\}[PW_{12}O_{40}]_2$ composed of two interpenetrating frameworks and polyoxometalate species.

Reproduced from Ref. [50] with permission from Nature Publishing Group© 2010.

usually lie on a common parallel plane. These arrays are always (4, 4) or (6, 3) layers linked by the polyoxoanions to generate a layer with a certain thickness. Then they mechanically intertwine, giving rise to a 3D mechanically interlocked network. In these species, there is an increase of dimensionality (2D → 3D). The other modes consisting of two identical sets of 2D layers spanning two different stacking directions, show an increase of dimensionality (2D → 3D), will also be discussed.

In 2010, Chen and co-workers reported the compound, $[Cu^{II}(btp)_2(H_2O)][\beta\text{-}Mo_8O_{26}]_{0.5}\cdot 2H_2O$ (**28**) [52], which displayed (2D → 3D) polycatenation based on (4, 4) layers with a certain thickness. In this species, the 2D layers are mechanically interlocked through polycatenation, giving rise to a well-defined 3D mechanically interlocked network as defined by this review. Each Cu^{II} ion is linked to four neighboring Cu^{II} ions through four btp ligands to form a 2D grid layer along the *ab* plane. Between adjacent layers, the β-$[Mo_8O_{26}]^{4-}$ anions, as pillars, are sandwiched to form a pillar-layered sheet. Each pillar-layered sheet, extending along the *ab* plane, is interlocked in a parallel fashion with the two nearest neighboring ones to give rise to a 3D polycatenated framework. In 2011, a similar structure was found in compound $[Cu^{II}(btp)_2(H_2O)(\beta\text{-}Mo_8O_{26})_{0.5}]\cdot H_2O$ (**29**) [53] (Fig. 6b) reported by You et al.

In 2012, Ma and co-workers reported a (2D → 3D) polycatenation structure $[Ag_6(Tipa)_4(\beta\text{-}Mo_8O_{26})][H_2(\beta\text{-}Mo_8O_{26})]\cdot 5H_2O$ (**30**) [54] based on (6, 3) layers. In compound **30**, Ag(I) atoms are linked by the two Tipa ligands generating into a 2D (6, 3) Ag-Tipa sheet. β-$[Mo_8O_{26}]^{4-}$ polyanions pillar two adjacent Ag-Tipa sheets to

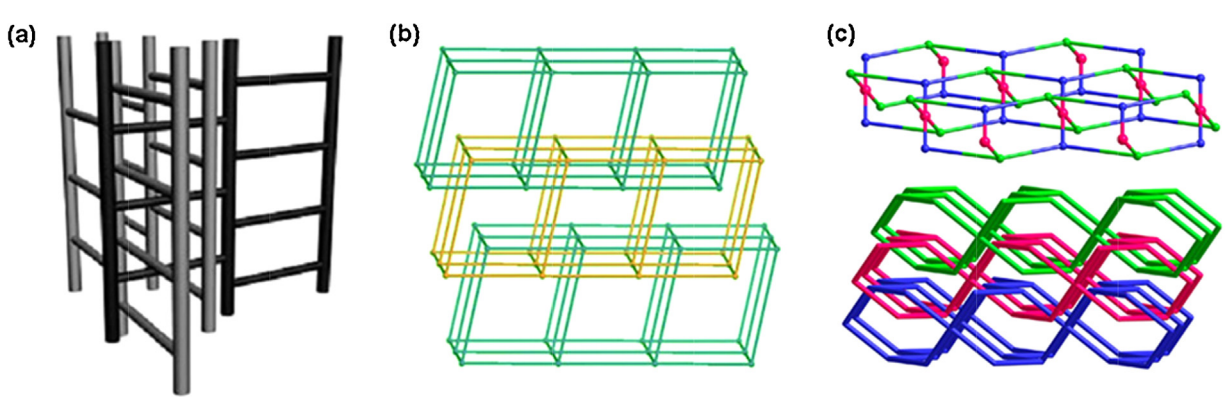

Fig. 6. (a) Schematic illustration of the (1D → 3D) polycatenated structures in compound **27**. (b) In compound **29**, 2D layer are mechanically interlocked in a parallel fashion with the two nearest neighboring ones giving a (2D → 3D) polycatenated structure. (c) Schematic representation of the trinodal (3,4)-connected net of **31**, and view of the (2D → 3D) polycatenated framework.

Reproduced from Refs. [51,55] with permission from John Wiley and Sons© 2006 and ACS© 2013.

generate a 2D double undulating layer with a 3-connected 8^3 net. Pairs of layers interpenetrate each other in a parallel fashion resulting in a 2-fold (2D → 2D) interpenetrating layer. The 2-fold interpenetrated layer is further catenated to the two adjacent such layers in parallel fashion to give an overall unique (2D → 3D) polycatenated framework. In the resulting array, each layer is interlocked with five others, with one on the same average plane, plus two of the four "above" and two "below" the layer.

On the other hand, the 2D motif can also have an irregular shape. An appropriate (2D → 3D) polycatenated example of this type is represented by $[Cu^I{}_4(L3)_4Mo_6O_{18}(O_3AsPh)_2]$ (**31**) [55] reported by Ma and co-workers in 2013. In this compound, Cu1, Cu2 and their symmetry-related species are linked alternatively by two kinds of L3 ligands to generate a helix chain. Each $[Mo_6O_{18}(O_3AsPh)_2]^{4-}$ polyoxoanion joints four Cu^I cations from four parallel helix chains to yield a 2D double-layer structure. The most fascinating and peculiar structural feature of **31** is that each double-layer is interlocked by the two nearest neighboring ones to form a 3D polycatenated framework (Fig. 6c).

A novel compound $[Cu_2(bpp)_4(H_2O)_2](SiW_{12}O_{40})\sim 6H_2O$ (**32**) [56] exhibits an inclined catenation of (4, 4) layers, in which the alternate Cu atoms connect bpp ligands to form a unique 2D grid-like cationic framework. The most interesting feature of **32** is that these 2D frameworks are stacked together to generate a 3D interpenetrating porous network, where $[SiW_{12}O_{40}]^{4-}$anions act as templates and are not coordinated to copper atoms.

From compound **27** to compound **30**, Keggin or $[Mo_8O_{26}]^{4-}$ anions all act as linkers; they connect the already-formed chains or layers to generate a ladder or pillar-layered sheet which can interlock with the neighboring ones to form a polycatenated structure. In agreement with the strict definition of polycatenation, the resultant networks all present an increased dimensionality compared with the constituent motifs. In the examples of compound **26** and compound **32**, the Keggin polyanions function as templates to help the formation of the polycatenated framework. Furthermore, evidence of an anion template effect is obvious in compound **26**. Without the presence of the Keggin polyoxometalate, the self-assembly of Ag^+ cations and 1,2,4-triazole leads to the formation of a two-dimensional $[Ag(trz)]_\infty$ network, not the 3D polycatenated architecture described above.

4. Polyrotaxane and poly*pseudo*-rotaxane in POM-based coordination polymers

A great deal of attention has been turned to a burgeoning family of entangled networks called polythreaded coordination networks. As described previously by Ma and Ciani et al., polythreaded systems are polymeric analogs of molecular rotaxanes and *pseudo*-rotaxanes; numerous fascinating topologies have been observed in these structures. Then admirable synthetic strategies initiated by Kim, Robson and others have been developed to assemble rotaxanes into polyrotaxanes which leads to a new field of polyrotaxane frameworks. Both polyrotaxanes and poly*pseudo*-rotaxanes contain closed two-membered rings/loops and rod/string elements that thread through the loops. The only difference between them is that in polyrotaxanes, both ends of the rod/string have capping groups (similar to a dumbbell) making the motifs inseparable without breaking links, whereas the rod/string may slip off and disentangle due to the absence of capping groups in poly*pseudo*-rotaxanes [23].

In other words, we can differentiate the known examples into two classes based on the possibility of extricating the components. One class consists of an extended system that 'cannot be disentangled' matching the definition of polyrotaxanes. The other is an entangled array containing 'separable' motifs which have characteristics of poly*pseudo*-rotaxane motifs. In some studies, the term polythreading is often used to describe the entangled characters of one compound, but in most cases, polythreading is always equivalent to poly*pseudo*-rotaxane. So we only use the term poly*pseudo*-rotaxane to describe the entangled characteristics of compounds for clarity in this paper.

4.1. Polyrotaxanes in POM-based coordination polymers

A few interesting POM-based coordination polymers exhibiting polyrotaxane network architectures have been reported so far. The alternating rings and rods in these compounds are particularly suitable for polythreading since they are the elements needed for rotaxane-like mechanical linkages. The resultant network can present equal or greater dimensionality than the constituent polythreading motifs. This type of entanglement yields (1D → 2D), (2D → 2D) and unusual 3D POM-based polyrotaxane frameworks.

In 2012, Wang et al. reported two interesting isostructural 1D → 2D polyrotaxane compounds $[Cu_2(L4)_3(SiMo_{12}O_{40})(H_2O)_6]\cdot 9H_2O$ (**33**) and $[Cu_2(L4)_3(SiW_{12}O_{40})(H_2O)_6]\cdot 6H_2O$ (**34**) [57]. As shown in Fig. 7a in compound **33**, the two Cu1 centers are linked by two L4 ligands with a "V"-type conformation to form a square $Cu_2(L4)_2$ loop. The other L4 ligands serve as bidentate ligands to bridge adjacent $Cu_2(L4)_2$ loops into a 1D chain. A closer inspection reveals that 1D chains in one position are molecular "strings" that pass through the "loops" of the 1D chains in another position to form a 1D→2D polythreading structure, further giving rise to a 2D polyrotaxane layer. Intriguingly, the $[SiMo_{12}O_{40}]^{4-}$ anions act as templates sandwiched between the neighboring polyrotaxane layers, resulting in an unprecedented 2D POM-based metal-organic polyrotaxane framework.

By reacting $(NH_4)_6Mo_7O_{24}\cdot 4H_2O$, CuCl and L5 at pH 5.9, Su et al. obtained one 2-fold (2D → 2D) interpenetrating host–guest network $[Cu^I{}_3(L5)_2(Mo_8O_{26})_{0.5}Cl]$ (**35**) [58]. Each L5 molecule acts as a bis-monodentate ligand, coordinating to two Cu^I cations, and every Cu^I cation is coordinated by two L5 molecules so as to form a window-like metal-organic closed loop. Every two Cu—Cl bonds bridge the closed loop into an infinite chain, and adjacent metal-organic rings are connected by a β-$[Mo_8O_{26}]^{4-}$ anion through Cu—O covalent bonds, which gives rise to a 2D layer. Fascinatingly, β-$[Mo_8O_{26}]^{4-}$ polyoxoanions link adjacent metal-organic closed loops in one layer, but it also threads through another loop from the adjacent layer, which is considered a host, in an inclined way to form the polythreading structure, further giving rise to a 2-fold 2D → 2D polyrotaxane host–guest network (Fig. 7b).

By reacting $Cu(NO_3)_2\cdot 3H_2O$, L6, and $H_3PMo_{12}O_{40}$, Wang and Su obtained another interesting complex, $[Cu^{II}(L6)_2(H_2O)_2][Cu^I{}_2(L6)_2]PMo_{12}O_{40}$ (**36**) [59] revealing a new type of 3D metal-organic polyrotaxane framework. Each Cu^{II} center is bridged to four adjacent metal centers through L6 ligands in boat conformations to form a typical diamondoid framework. Because of the spacious nature of a single network, it allows a second identical diamondoid network to penetrate it in a normal mode, thus giving a 2-fold interpenetrated structure. Such a crystal structure with extra-large pores is still unstable unless there are suitable guests or further interpenetration occurs. This need is fulfilled by another entanged structure. Two Cu^I centers are linked by two L6 ligands to form a 34-membered macrocycle. These cycles interlock the formed 2-fold interpenetrated diamondoid network in a unique pattern, not by the common interpenetration, but rather by the unusual rotaxane mode. Keggin ions are encapsuled in the host framework and have a weak interaction with Cu1 atoms to stabilize the whole crystal structure (Fig. 7c).

In the cases mentioned above, the β-$[Mo_8O_{26}]^{4-}$ polyoxoanion acts as a linker in compound **35**, connecting adjacent metal–organic closed loops, while Keggin polyoxometalates in compound **33** and

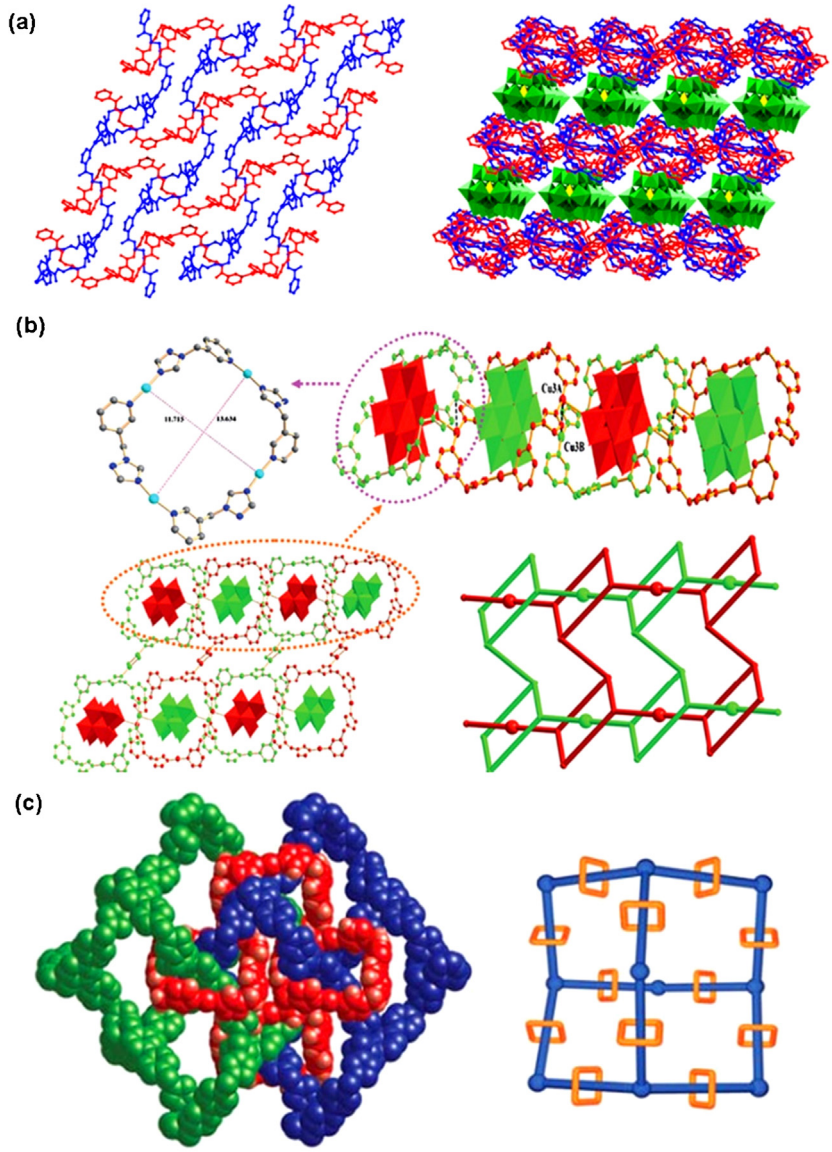

Fig. 7. (a) The $[SiMo_{12}O_{40}]^{4-}$ anions sandwiched by neighboring parallel-packed 2D polyrotaxane layers in **33**. (b) Schematic representation of the 2D → 2D polythreading interpenetrating network in **35**. (Adjacent layers are, in red and green, respectively.) (c) Schematic representation of the two interpenetrating diamondoid units (green and blue) interlocked by molecular squares (red) and the adamantanoid cage locked by twelve molecular squares in compound **36**.
Reproduced from Refs. [58,59] with permission from RSC© 2007 and 2010.

36 both act as templates to help the formation of the more sophisticated architectures.

4.2. Polypseudo-rotaxane in POM-based coordination polymers

Motifs of this second type are threaded by chains or strings which, in principle, can be slipped off without breaking links. This type of polythreading is called poly*pseudo*-rotaxane. Furthermore, in the cases of POM-based coordination polymers, the threading elements are usually the infinite chains composed of metal and ligands. The constituent units could have 0D, 1D or higher dimensionalities and the resultant network can present equal or greater dimensionality than that of component motifs. So in this section, we will describe the compound according to the combination pattern of their single motifs, and classify them into four categories: 3D + 1D (Section 4.2.1), 2D + 1D (Section 4.2.2), 1D + 1D (Section 4.2.3) and 0D + 1D (Section 4.2.4).

4.2.1. Polypseudo-rotaxane based on 3D + 1D mode

In 2008, Lan et al. reported an interesting 3D poly*pseudo*-rotaxane architecture with 3D framework and 1D polymeric chain $[Cu^{II}(bbi)_2(\alpha\text{-}Mo_8O_{26})][Cu^{I}(bbi)]_2$ (**37**) [33]. In compound **40**, the bbi ligands link Cu^{II} cations to generate a 2D (4, 4) sheet with the dimensions of 13.5 Å × 14.1 Å, and each α-$[Mo_8O_{26}]^{4-}$ anion links two Cu^{II} cations from different layers to form a 3D **pcu** topological framework. Another type of bbi ligand forms a $[Cu^{I}(bbi)]^{+}$ chain combined with Cu^{I} cations. As a result, an unusual 3D polythreaded framework is formed by two chains threading through the distorted **pcu** skeleton (Fig. 8a). Compound $[Cu^{II}Cu^{I}(bbi)_3(\alpha\text{-}Mo_8O_{26})][Cu^{I}(bbi)]$ (**38**) [33] has an almost identical structure to **37** except it contains a different 3D framework with 6-connected **pcu** topology. If $Cu^{I}\cdots O$ interactions are considered, the structure of compound **37** is a novel self-penetrating (3,4,6)-connected framework with $(5^2{\cdot}8)_2(5^4{\cdot}6{\cdot}8)(4^4{\cdot}6^{10}{\cdot}10)$ topology, and the structure of compound **38** is a normal 3D (4,6)-connected framework with $(4^2{\cdot}6^3{\cdot}7)(5\cdot6^4\cdot8)(4^2\cdot5^6\cdot6^6\cdot8)(4^2\cdot5^6\cdot6^4\cdot7\cdot8^2)$ topology.

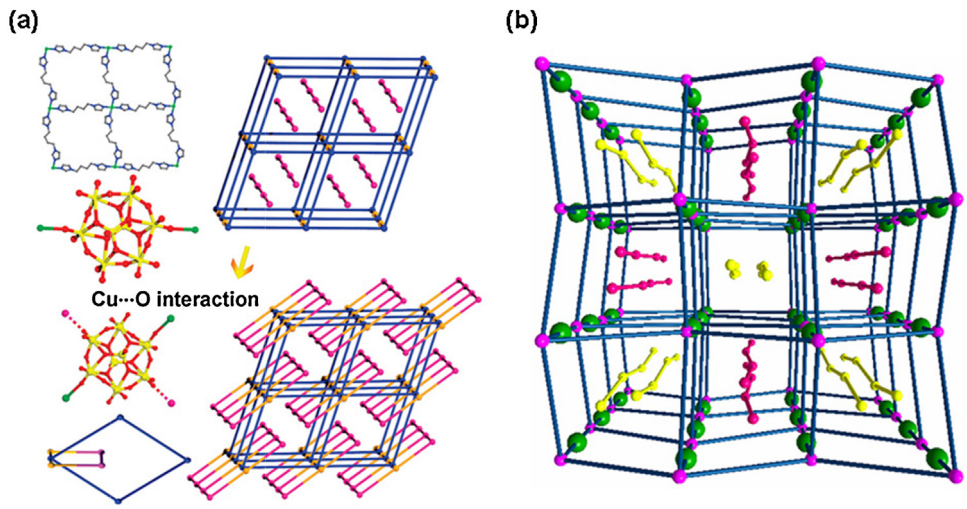

Fig. 8. (a) Schematic view of the 3D poly*pseudo*-rotaxane framework of compound **37** and the self-penetrating (3,4,6)-connected framework with $(5^2\cdot 8)_2(5^4\cdot 6\cdot 8)(4^4\cdot 6^{10}\cdot 10)$ topology in compound **37** (the $Cu^{I}\cdots O$ interactions being considered). (b) Schematic representation of a poly*pseudo*-rotaxane framework in compound **43**. Reproduced from Refs. [33,61] with permission from ACS© 2008 and RSC© 2008.

Similar complexes that exhibit the same entangled topology of 3D + 1D poly*pseudo*-rotaxane architecture include: $[Cu^{I}(bix)][(Cu^{I}bix)(\delta\text{-}Mo_8O_{26})_{0.5}]$ (**39**) [60], $H(Cu^{I}bix)[(Cu^{I}bix)_2(\beta\text{-}Mo_8O_{26})]\cdot 2H_2O$ (**40**) [60] and $[M_4(bix)_4][\delta\text{-}Mo_8O_{26}]$ [M = Cu (**41**), Ag (**42**)] [32].

The 3D + 1D mode of poly*pseudo*-rotaxane can also lead to a chiral structure upon crystallization without any enantiopure chiral auxiliary. In 2008, Lan et al. obtained one chiral compound $[Cu(bbi)_2V_{10}O_{26}][Cu(bbi)]_2\cdot H_2O$ (**43**) [61] constructed from achiral bbi ligands and high symmetry $[V_{10}O_{26}]^{4-}$ polyoxoanions (Fig. 8b). The bbi units act as bis-monodentate bridging ligands, and coordinate to Cu1 ions to generate a 2D waved (4, 4) sheet, which is pillared by $[V_{10}O_{26}]^{4-}$ polyoxoanions to extend to a distorted 3D **pcu** topological framework. Two Cu2–bbi chains pass through one channel, and two Cu3–bbi chains are inserted into another channel along the crystallographic *c* axis. Thus, the distorted **pcu** skeleton is threaded by two helical chains composed of the achiral ligand bbi and different Cu atoms resulting in an unusual chiral 3D poly*pseudo*-rotaxane framework.

4.2.2. Polypseudo-rotaxane based on 2D + 1D mode

In the species mentioned above, the phenomenon of poly*pseudo*-rotaxane does not affect the dimensionality of the resultant network. In some other cases, the entanglement of poly*pseudo*-rotaxane motifs can lead to an increased dimensionality via polythreading of different components, although most of them are supermolecular structures.

In this type there are two crystallographically independent and distinct polymeric motifs: one-dimensional (1D) S-shaped chain and the two-dimensional (2D) undulated layer. The S-shaped chains penetrate into the 2D parallel layers to generate an unusual 2D + 1D → 3D poly*pseudo*-rotaxane framework.

In 2006, parallel threading of 1D chains into undulated 2D (4, 4) sheets in compound $[Cd(BPE)(\alpha\text{-}Mo_8O_{26})][Cd(BPE)(DMF)_4]\cdot 2DMF$ (**44**) (DMF = *N*,*N*-dimethylformamide) was observed by Liao and co-workers [62]. In the 2D $[Cd(BPE)(\alpha\text{-}Mo_8O_{26})]_n^{2n-}$ frameworks, each Cd^{2+} ion is in an octahedral environment, with two axial sites bound to two BPE ligands, and the equatorial sites bound to two $\alpha\text{-}[Mo_8O_{26}]^{4-}$ clusters in an unprecedented bonding mode. Thus, each octamolybdate uses two opposite pairs of oxo groups to coordinate two Cd^{2+} ions, respectively. In 1D $[Cd(BPE)(DMF)_4]_n^{2n+}$, each Cd^{2+} ion is coordinated by four DMF as ligands, and these Cd^{2+} ions are then bridged by BPE ligands to extend into infinite chains that penetrate into the mesh of $[Cd(BPE)(\alpha\text{-}Mo_8O_{26})]_n^{2n-}$ sheets to yield a 2D + 1D → 3D poly*pseudo*-rotaxane framework (Fig. 9a).

In most instances, the 2D motifs do not always have a regular construction. In 2013, Ma and co-workers reported a fascinating framework $[Cu^{I}_2(cis\text{-}btp)_2][Cu^{I}_2(trans\text{-}btp)_2Mo_6O_{18}(O_3AsPh)_2]$ (**45**) [55]. In this case, the cis-btp ligands bridges neighboring Cu^{I} atoms to form the first 1D S-shaped $[Cu_2(cis\text{-}btp)_2]^{2+}$ motif, while the trans-btp ligands and the bidentate $[Mo_6O_{18}(O_3AsPh)_2]^{4-}$ anions link the adjacent Cu^{I} atoms into the second 2D $[(Cu1)_2(trans\text{-}btp)_2(As_2Mo_6)]^{2-}$ motif. Strikingly, the S-shaped chains penetrated into the 2D parallel layers to generate an unusual 1D + 2D → 3D framework. From a topological standpoint, this unusual 3D array belongs to poly*pseudo*-rotaxane architecture (Fig. 9c). It is noteworthy that the structure of compound **45** is different from the previously reported 3D poly*pseudo*-rotaxane architecture. In this compound, the layer exhibits a wavelike brick-wall (6, 3) network and it is penetrated by a 1D chain in two different directions.

Other related complexes $[Cu(bbi)]_2[Cu_2(bbi)_2(\delta\text{-}Mo_8O_{26})_{0.5}]\text{-}[\alpha\text{-}Mo_8O_{26}]_{0.5}$ (**46**) (Fig. 9b) [63], $[Cu(bbi)][Cu(bbi)(\theta\text{-}Mo_8O_{26})_{0.5}]$ (**47**) (Fig. 9d) [63], $[Na_2(H_2O)_8Ag_2(HINA)_3(INA)][Na(H_2O)_2Ag_2\text{-}(HINA)_4(H_2W_{12}O_{40})]\cdot 2H_2O$ (**48**) [64], $[Cu(L1)]_4[SiMo_{12}O_{40}]$ (**49**) [65], $[Cu(L6)_2(HPW^{VI}{}_{10}W^{V}{}_2O_{40})][Cu(L6)(H_2O)_4]\cdot 4H_2O$ (**50**) [66] and $[Ag_5(L7)_5][K_2(OH)P_2W_{18}O_{62}]\cdot H_2O$ (**51**) [67] also exhibit a similar entangled architecture.

4.2.3. Polypseudo-rotaxane based on 1D + 1D mode

In 2009, an interesting 3D poly*pseudo*-rotaxane architecture with 1D polymeric chains penetrating 1D ladders $[Cu_4(L1)_4][\beta\text{-}Mo_8O_{26}]_{0.5}[\gamma\text{-}Mo_8O_{26}]_{0.5}\cdot H_2O$ (**52**) was reported by Xu and coworkers [32]. A solution of long spacer ligand L1, $Cu(CH_3COO)_2\cdot H_2O$ and $Na_2MoO_4\cdot H_2O$ generates complex **52**. All of the Cu(1) centers are joined together by the L1 molecules to generate an infinite $[Cu\text{–}L1]_n$ thread (labeled as thread A). The alternate Cu (4) and Cu (5) centers are also linked together by L1 to form another $[Cu\text{–}L1]_n$ thread (labeled as thread B). Interestingly, the two types of Mo_8 anions, functioning as the rungs, bridge two sets of $[Cu\text{–}L1]_n$ polymeric single chains made from Cu(2)–L1 and Cu(3)–L1 fragments, respectively, to form two types of ladder-like double chains of $[Cu(2)(L1)(\gamma\text{-}Mo_8)_{0.5}]_n^{n-}$ (labeled as ladder A) and $[Cu(3)(L1)(\beta\text{-}Mo_8)_{0.5}]_n^{n-}$ (labeled as ladder B), The most

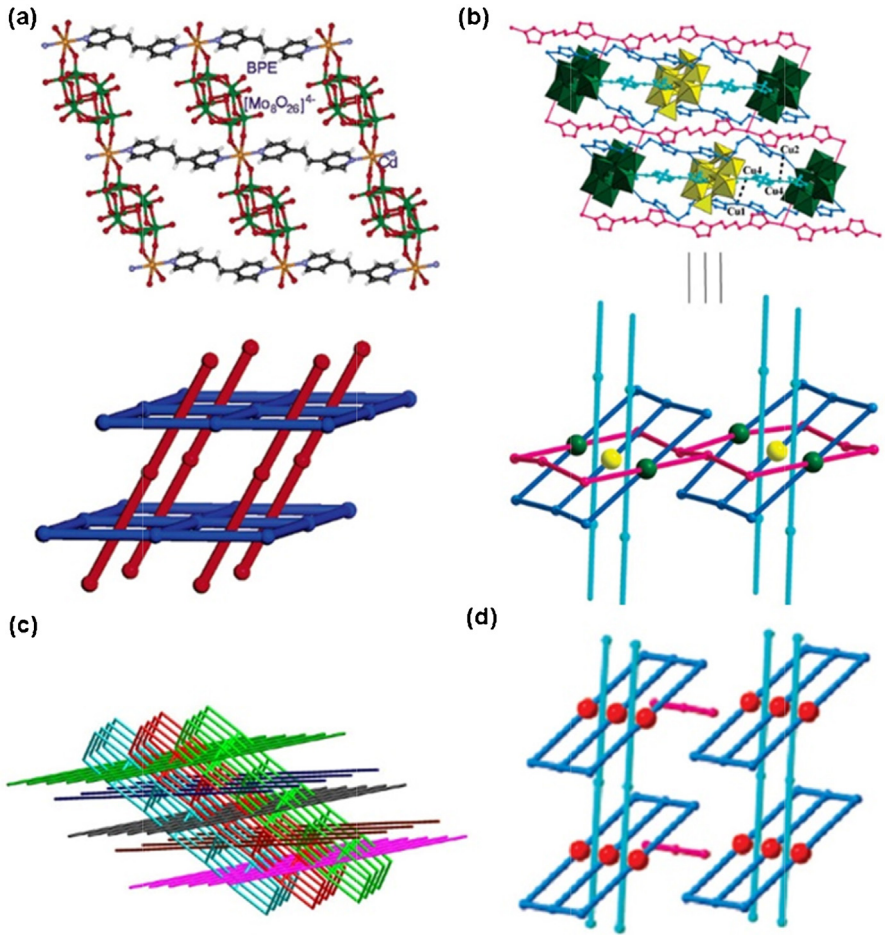

Fig. 9. (a) Schematic representation of $[Cd(BPE)(DMF)_4]_n^{2n+}$ chains (in red) penetrating $[Cd(BPE)(\alpha\text{-}Mo_8O_{26})]_n^{2n-}$ grids (in blue) in **44**. (b) Schematic representation of the poly*pseudo*-rotaxane structure in **46**. (c) Schematic representation of the 3D poly*pseudo*-rotaxane framework in **45**. (d) Schematic representation of the poly*pseudo*-rotaxane structure in **47**.

Reproduced from Refs. [55,62,63] with permission from ACS© 2006, 2008 and 2013.

fascinating structural feature of **52** is that those two ladders, ladder A and ladder B, are penetrated respectively by single-stranded thread B and double-stranded thread A in an inclined way. Two such types of polythread-penetated subunits array alternately in a crosslike fashion (Fig. 10a).

Another example of this mode can be found in compound $[Ag_{0.52}Na_{0.48}(\beta\text{-}Mo_8O_{26})(H_2O)][Ag_3(Tipa)_2]$ (**53**) [54]. In 2012, Ma and co-workers reacted $AgNO_3$, Tipa, $(NH_4)_6Mo_7O_{24}{\cdot}4H_2O$ and water with pH ≈ 1, and succeeded in crystallizing compound **53**. In this case, each crystallographically half-occupied Ag1 ion binds two

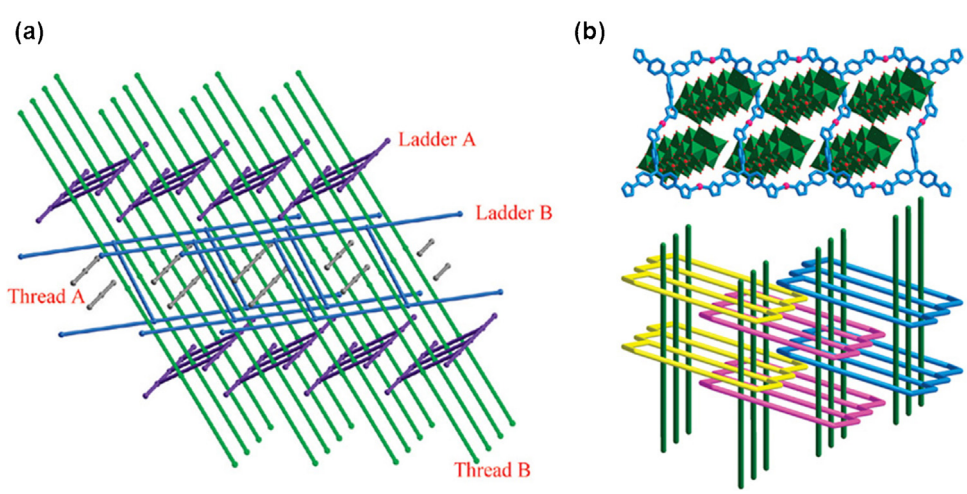

Fig. 10. (a) View of the poly*pseudo*-rotaxane structure in compound **52**. (b) View and the schematic representation of the $1D_{ladder} + 1D_{chain} \rightarrow 3D_{poly\textit{pseudo}\text{-rotaxane}}$ framework in compound **53**.

Reproduced from Refs. [32,54] with permission from ACS© 2009 and 2012.

adjacent β-$[Mo_8O_{26}]^{4-}$ clusters through four Ag – O bonds from two $[O_4]$ faces of two Mo_8 clusters, resulting in an infinite inorganic anion chain of $[Ag_{0.52}Na_{0.48}(\beta\text{-}Mo_8O_{26})(H_2O)]^{3-}$. Each Tipa ligand links the adjacent Ag2 and Ag3 atoms to generate a cationic 1D ladder of $[Ag_3(Tipa)_2]^{3+}$. The rectangular opening is divided into two infinite rectangular channels by the ladders located above and below. These channels in turn are occupied by the inorganic chains, in which one rectangular opening is filled by two cationic chains to generate a novel $1D_{ladder} + 1D_{chain} \rightarrow 3D_{poly\textit{pseudo}\text{-rotaxane}}$ framework (Fig. 10b).

Another 3D supramolecular complex also has the 1D + 1D poly*pseudo*-rotaxane architecture; (bix)[Cu(bix)][Cu_2(bix)$_2$-($P_2W_{18}O_{62}$)]·2H_2O (**54**) [68] is composed of two 1D motifs, in which one 1D metal-ligand chain threads through the formed macrocycles to form a sheet with the poly*pseudo*-rotaxane structure.

4.2.4. Polypseudo-rotaxane based on 0D + 1D mode

A related complex $[Ag(L1)]_4[SiMo_{12}O_{40}]\cdot 2H_2O$ (**55**) [65] was reported by Xu and co-workers in 2009. Every other Ag(1) center is connected through two V-shaped L1 molecules to form a dinuclear molecular loop of $[Ag(1)(L1)_2]^{2+}$. Ag(2) and Ag(3) centers are bridged by the Z-shaped L1 molecules to form two kinds of wavelike chains of $[Ag(2)(L1)]_n^{n+}$ and $[Ag(3)(L1)]_n^{n+}$, respectively. Uncoordinated $[SiMo_{12}O_{40}]^{4-}$ polyoxoanions acting as templates induce a kind of wavelike chain of $[Ag(2)(L1)]_n^{n+}$ to surround them with short contact interactions, forming a polyoxoanion-templated layer structure. Poly*pseudo*-rotaxane structural character is observed between the binuclear molecular loop and wavelike chain $[Ag(3)(L1)]^+$. In the lattice, the $[SiMo_{12}O_{40}]^{4-}$-templated supramolecular layers and the 0D + 1D poly*pseudo*-rotaxane polymers are interlaced and interact via short contact interactions between polyoxoanions and the $[Ag(3)(L1)]^+$ chain.

In 2010, Peng and Su successfully isolated an interesting 3D compound $[Cu(L8)]_2(HPW_{12}O_{40})\cdot 3H_2O$ (**56**) [69] through combination of $H_3[PW_{12}O_{40}]\cdot 12H_2O$, $Cu(CH_3COO)_2\cdot H_2O$, and L8. One structural feature of compound **56** is the unusual 3D metal–organic *pseudo*-rotaxane framework connected by the 0D 34-membered macrocycles (motif II) acting as molecular "loops" and the 1D chain (motif I) serving as a long molecular "string". Consequently, a complicated 3D metal-organic *pseudo*-rotaxane framework is formed by repeating this interesting entangled pattern. This entanglement is rare in previous reports on *pseudo*-rotaxane structures, namely, one "loop" encircles two "strings" rather than a single one. Topological analysis shows that this framework can be described as a 2-fold **dia** net if we take the two "strings" in one "loop" as a node. Another fascinating structural feature of compound **56** is its highly open 3D metal-organic *pseudo*-rotaxane framework. The *pseudo*-rotaxane motifs composed of $[Cu(L8)]^+$ chains, and $[Cu_2(L8)_2]^{2+}$ macrocycles are hexagonally arranged to construct hexagonal 3D channels. The cylinder-like channels are so large that the Keggin $[PW_{12}O_{40}]^{3-}$ anions are accommodated as charge-compensating guests (Fig. 11).

In 2012, Zhang and co-workers described an interesting 3D poly*pseudo*-rotaxane complex [(AgL7)$_2$-Ag$_2$(L7)$_2$][($SiW_{12}O_{40}$)] (**57**) [67]. In the framework, the 0D $[Ag_2(L7)_2]_n^{2n+}$ circle acts as a molecular "loop", and the 1D $[(AgL7)_2]_n^{2n+}$ chain serves as a long molecular "string". Then each "string" threads through a "loop" and each "loop" encircles a "string", forming a 1D poly*pseudo*-rotoxane motif. The Ag chains go through the poly*pseudo*-rotoxane motifs, connecting the "loops" and "strings" to a 2D novel layer framework. Furthermore, the Keggin clusters act as templates, located between the 2D layers and connecting the adjacent layers to a 3D POM-based network.

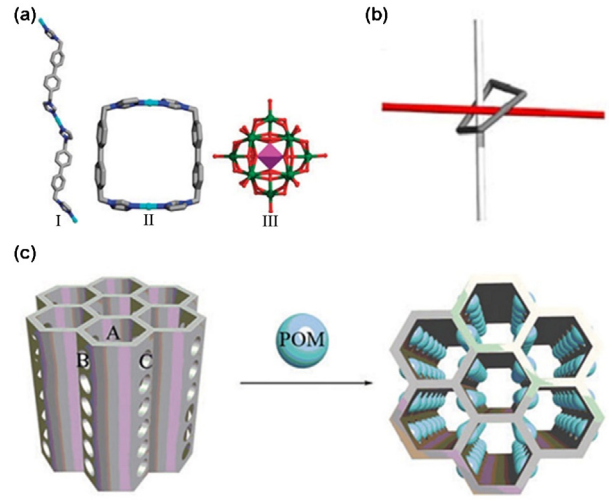

Fig. 11. (a) The three crystallographically distinct motifs in compound **56**. (b) The unusual intercalated fashion of two "strings" in one "loop". (c) Schematic representation of the model and arrangement of POMs in the tunnels.
Reproduced from Ref. [69] with permission from RSC© 2010.

In Section 4.2, complexes with poly*pseudo*-rotaxane architectures have been classified into four types: 3D + 1D, like those seen in compounds **37**–**43**, where the phenomenon of poly*pseudo*-rotaxane does not affect the dimensionality characteristic of the resultant network. The POMs always act as linkers to generate the 3D framework, which is penetrated by metal-ligand chains to give the 3D + 1D poly*pseudo*-rotaxane structure. Next, the 2D + 1D and 1D + 1D types, in which the entanglement of poly*pseudo*-rotaxane motifs leads to a dimensional increasing via polythreading of different components. In these cases, POMs function as linkers to produce the layers or the chains, and the different shaped chains penetrated into the parallel layers or ladders to generate an increased dimensionality framework. At last, in 0D + 1D, POMs usually act as templates, like the structures in compound **55**–**57**. The POMs are usually located between the 2D layers or in the 3D frameworks, and help to form a relatively high dimensional POM-based network.

4.3. Coexistence of polycatenation and polyrotaxane characteristics

In addition, there are also some entangled networks with characteristics of both polycatenation and polyrotaxane coordination polymers. This particular type is rare in POM-based coordination polymers; only five examples have been reported thus far.

In 2008, L1 with $Cu(NO_3)_2\cdot 3H_2O$, $H_3PMo_{12}O_{40}$ and NH_4VO_3 were reacted under hydrothermal conditions, and an unusual 3D POM-based framework $[Cu^I{}_3(L1)_3][\{Cu^{II}(L1)_2\}\{PMo_{12}O_{40}(VO)_2\}]\cdot H_2O$ (**58**) was achieved by Wang et al. [70]. In compound **58**, the first 2D loop-containing network is constructed from two types of L1 ligands and two crystallographically independent Cu(I) atoms. The second motif is a single 3D framework. In the 3D net, each Cu(II) atom is connected to four adjacent ones through four L1 ligands to yield a 2D network which is then cross-linked by bicapped Keggin polyoxoanions to give a single 3D **pcu** framework (Fig. 12). The most outstanding structural feature of compound **58** is that the loop-containing 2D layers are inextricably entangled with the 3D frame in an intricate, unprecedented manner, displaying the polyrotaxane/polycatenane associations.

In 2009, Xu and co-workers reported compounds $[M_2(H_2O)_4(L1)_3][SiMo_{12}O_{40}]\cdot 4H_2O$ (M = Mn (**59**), Ni (**60**) and Co (**61**)) [65], which showed 2D interpenetrated networks featuring both polyrotaxane and polycatenane traits. Only the structure of

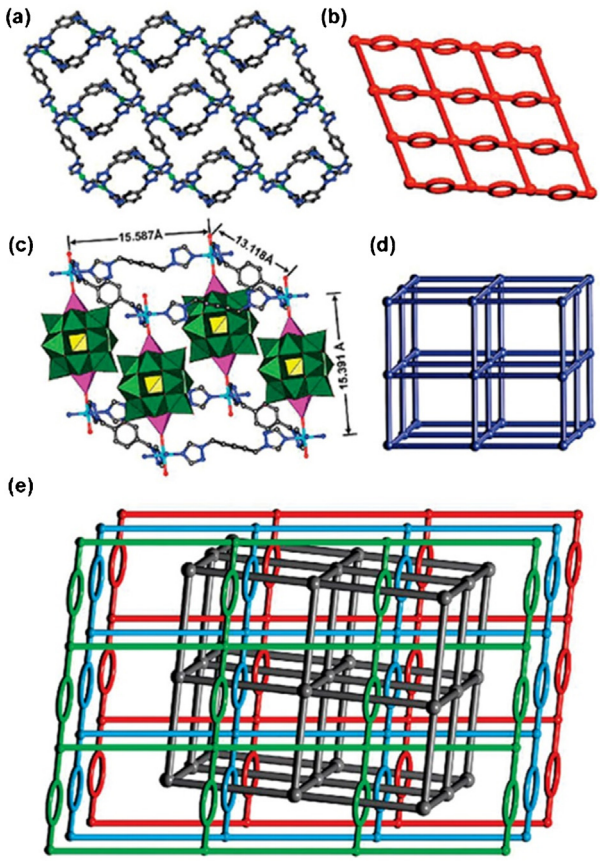

Fig. 12. The two different motifs in **58**: (a) chemical and (b) schematic views of the 2D loop-containing network, (c) chemical and (d) schematic views of the 3D **pcu** net, and (e) a schematic view of the overall 3D framework displaying the polyrotaxane/polycatenane characteristics in **58**.

Reproduced from Ref. [70] with permission from ACS© 2008.

compound **59** is described here in detail because the other two are isomorphic structures to compound **59**. In compound **59**, two V-shaped L1 molecules together with two Mn^{2+} ions constitute one type of $[Mn_2(L1)_2]^{4+}$ dinuclear molecular loop. Each $[SiMo_{12}O_{40}]^{4-}$ cluster is bridged by two $[Mn_2(L1)_2]^{4+}$ loops to form an 1D extension. The Z-shaped L1 molecules are arranged perpendicularly to the direction of the chain propagation and extend the chains into a 2D net with quadrate channel. Two such nets penetrate each other with each loop in one layer threaded by rods of the other layer so as to form a 2-fold parallel-interpenetrated network with a polyrotaxane nature. Furthermore, the 2-fold nets also exhibit polycatenane behavior as the smallest rings of one net are involved in catenane associations with the second-smallest rings of the other net (Fig. 13). Then the 2-fold nets pack along the *b* axis of the crystal via extensive O—H···O hydrogen bond interactions.

Another example belonging to this classification was reported by Lu and co-workers in 2011. In compound $Ag_{14}(trz)_{10}[SiW_{12}O_{40}]$ (**62**) [71], the entanglement exhibiting both polyrotaxane and polycatenane characteristics occurs in the formation of the 2D mechanically interlocked network. There are two kinds of the POMs in compound **62**, both exhibiting the role of templates.

5. Self-penetration in POM-based coordination polymers

Self-penetrating networks (also called self-catenating, self-entangling or polyknotting), are single nets which have a peculiar feature in which the topological rings are passed through (catenated) by other components from the same network. The number of identified self-penetrating structures in POM-based coordination polymers has risen in the past few years.

In 2008, Lan et al., for the first time, presented a chiral POM-based self-penetrating framework $[Ni_2(bbi)_2(H_2O)_4V_4O_{12}]\cdot 2H_2O$ (**63**) [72]. In **63**, V1 cations are linked to each other in corner-sharing modes to generate a $[(VO_3)^-]_8$ helical chain with a 4-fold screw axis along the *c* axis, and the V2 and V3 cations are linked each other in cornersharing modes to generate a $[(V_2O_6)^{2-}]_8$ helical chain, with a 2-fold screw axis along the *c* axis. The two kinds of helical chains are connected by Ni cations to form a 3D chiral inorganic skeleton. The bbi ligands link the Ni cations to generate chains, which interweave like the "warp" and "weft" along the *a* and *b* axes to form a molecular fabric structure. The inorganic skeleton and the molecular fabric structure described above are fused by sharing Ni centers to form a complicated 3D 3,4-connected chiral self-penetrating framework with $(7^2\cdot 8)(7^2\cdot 8^2\cdot 9^2)(7^3\cdot 8^2\cdot 10)$ topology. In this net, two crystallographically related rings with composition -Ni-bbi-VO_4-Ni-V_4O_{13}- are catenated with each other to give a self-penetrating (self-catenation or polyknotting) 3D structure (Fig. 14).

Also in the year 2008, Tian et al. reported another self-penetrating example based on Keggin-type anions. Compound $[Cu_5(btx)_4(PMo^{VI}{}_{10}Mo^{V}{}_2O_{40})]$ (**64**) [73] was obtained by the hydrothermal method in pH = 3.0. The compound $[Cu^{I}{}_5(btx)_4(PW^{VI}{}_{10}W^{V}{}_2O_{40})]$ (**65**) [74] which was also reported by Tian and co-workers is a topological isomorphic structure to compound **64**. In **64**, Cu1, Cu2, and Cu3 ions are viewed as two connecting nodes, respectively. With the connection of the ligands, a $(12^3)(12^1)_2$ Cu-btx layer is formed in a "grid" style. Interestingly, there are three sets of $(12^3)(12^1)_2$ 2D nets, which generate a 3-fold interpenetrating wave-like structure. The $[PMo^{VI}{}_{10}Mo^{V}{}_2O_{40}]^{5-}$ anion, acting as a hexadentate ligand, offers four terminal and two bridging O atoms to link the adjacent two interpenetrating

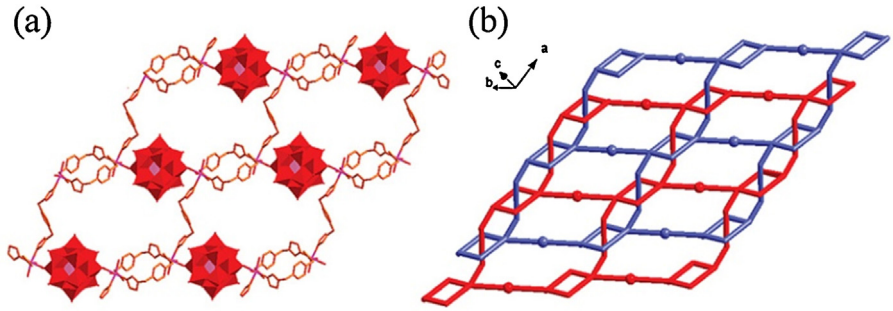

Fig. 13. (a) View of the 2D net constructed by $[Mn_2(L1)_2]^{4+}$ loops and $[SiMo_{12}O_{40}]^{4-}$ polyoxoanions. (b) Schematic illustration of the 2-fold parallel-interpenetrated network in compound **59**.

Reproduced from Ref. [65] with permission from ACS© 2009.

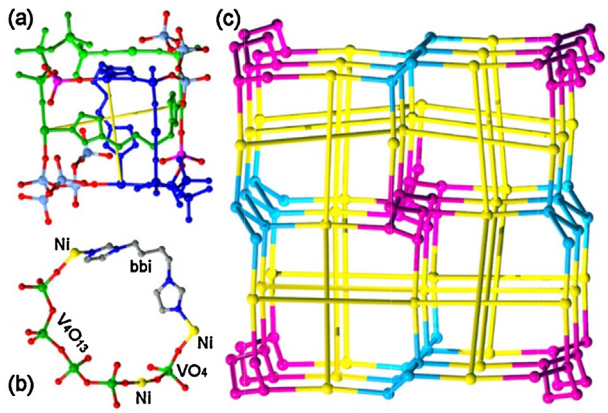

Fig. 14. (a) Ball-and-stick representations of the self-penetrating framework in compound **63**. (b) One ring with the composition -Ni-bbi-VO_4-Ni-V_4O_{13}- in the self-penetrating framework. (c) Schematic representation of the (3,4)-connected framework of compound **63**.

Reproduced from Ref. [72] with permission from John Wiley and Sons© 2008.

nets. Thus, the three interpenetrating Cu-btx nets are united by the $[PMo^{VI}{}_{10}Mo^{V}{}_{2}O_{40}]^{5-}$ anions to construct a 3D self-penetrating structure. Other self-penetrating compounds based on Keggin-type unit are compounds $[Cu^{I}{}_{12}(bmtr)_9(HSiMo_{12}O_{40})_4]$ (**66**) [75] and $[Ag_6Cl_2(mmt)_4(H_4SiMo_{12}O_{40})(H_2O)_2]$ (**67**) [76].

At the same time, Peng and co-workers reported another fascinating 3D self-penetrating network $[Cu_3(btx)_{5.5}(P_2W_{18}O_{62})]\cdot 4H_2O$ (**68**) [77]. In compound **68**, Cu1, Cu2, and Cu3 ions are viewed as three, four, and three connecting nodes, respectively, thus, a $(6^1\cdot 10^2)_2(6^1\cdot 8^2\cdot 10^3)$ 3D MOF is formed. Interestingly, there are two sets of these 3D nets, which generate a 2-fold interpenetrated structure. The $[P_2W_{18}O_{62}]^{6-}$ anion, acting as a five-connected ligand, offers three terminal O atoms to link one net and offers two terminal O atoms to link the other one. Thus, the two interpenetrated MOFs are united by the $[P_2W_{18}O_{62}]^{6-}$ anions to construct a 3D self-penetrating structure. Compounds $[Co_2(btb)_4(H_2O)][H_2P_2W_{18}O_{62}]\cdot 3H_2O$ (**69**) [78] and $[Co_2(btb)_4(H_2O)][H_2As_2W_{18}O_{62}]\cdot 6H_2O$ (**70**) [78] based on Dawson units also exhibit self-penetrating architecture.

In 2011, by combination of $H_3PMo_{12}O_{40}$, $Ni(NO_3)_2\cdot 6H_2O$ and BIMB ligand, Su et al. successfully isolated the 3D self-penetrating complex $[Ni_2(BIMB)_2(Mo^{VI}{}_4Mo^{V}{}_2O_{19})]$ (**71**) [79]. The nickel ion can be considered to be a six-connected node and $[Mo_6O_{19}]^{4-}$ anion as a four-connected node, so it is a 3D (4,6)-connected framework. Additionally, this framework displays a self-penetrating phenomenon, that is, the four-membered rings are catenated by the four-membered rings and six-membered rings belonging to the same framework, giving rise to the polycatenanes motifs (Fig. 15). This is the first (4,6)-connected binodal self-penetrating framework example reported for POM-based coordination polymers. Other self-penetrating compounds based on the Lindqvist unit are compounds $[(4,4'\text{-bpy})_6Cu^{I}{}_6Cl_3(Mo^{V}W_5O_{19})]$ (**72**) [43] and $[Cu^{I}{}_4(btb)_4Mo_6O_{18}(O_3AsPh)_2]$ (**73**) [55].

In 2011, another example of this class was observed in compound $[Zn(BIMB)_2(\gamma\text{-}Mo_8O_{26})_{0.5}]$ (**74**) (Fig. 16a) [34]. In compound **74**, when a Zn^{II} cation is regarded as a five-connected node and the γ-$[Mo_8O_{26}]^{4-}$ anion as a six-connected node, we obtained a (5,6)-connected topological structure with the short Schläfli symbol of $(4\cdot 5^7\cdot 6^2)_2(4^2\cdot 5^{11}\cdot 7^2)$. Furthermore, this framework displays a self-penetrating phenomenon, that is, the shortest four-membered rings are catenated by the six-membered rings belonging to the same framework, giving rise to a self-catenated motif. Other self-penetrating compounds based on the $[Mo_8O_{26}]^{4-}$ unit are compounds $[Cu_3(BIMB)_4(H_2O)(\delta\text{-}Mo_8O_{26})Cl_2]\cdot 3H_2O$ (**75**) (Fig. 16b) [34], $[Cu^{II}{}_2(btx)_4][\alpha\text{-}Mo_8O_{26}]$ (**76**) [80], $[Ag_2(2,4'\text{-tmbpt})_2(\alpha\text{-}Mo_8O_{26})_{0.5}(H_2O)_{0.5}]\cdot 2H_2O$ (**77**) [81], $[Ni(btb)_2(H_2O)][\gamma\text{-}Mo_8O_{26}]_{0.5}\cdot H_2O$ (**78**) [82] and $Cu^{I}{}_8(L1)_6[(\alpha\text{-}Mo_8O_{26})(\beta\text{-}Mo_8O_{26})]$ (**79**) [49].

As seen in the examples above, self-penetrating networks in POM-based coordination polymers are relatively common. POMs all serve as linkers and are regarded as nodes in the 3D framework, and the polythreading motifs are usually the organic ligands. But the formation of the structural diversities has a close relationship with the presence of the POMs; the various connection modes and strong coordination ability of the POMs allow for a variety of different self-penetrating networks.

As illustrated by the examples discussed above, POM-based coordination polymers can yield many types of entangled structures. The reasons why these fascinating entanglement characteristics exist in this kind of coordination polymer can be summarized as follows: (1) the coordination ability of the polyoxoanion to combine with different transition-metals makes them a good candidate to serve as inorganic linkers through their terminal and/or bridging oxygen atoms; (2) the high negative charges of the POMs help assemble cationic metal-organic subunits, making them outstanding anionic templates or charge-compensating guests that stabilize the whole framework; (3) the unique nano-sized polyoxometalate clusters usually have tunable shapes and sizes, such as Wells–Dawson (13.45 Å × 10.36 Å), Keggin (10.45 Å × 10.45 Å) and Anderson (9.07 Å × 9.07 Å) clusters, which result in the construction of different metal organic structures; (4) the coordination number of the POM can range from 1 to 12 or more theoretically, increasing the chemical variability and meanwhile being an important factor for the abundant structural diversity.

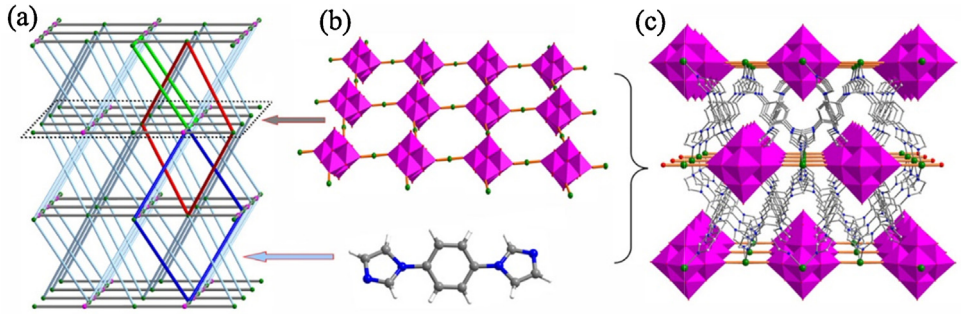

Fig. 15. (a) Schematic representation of the 3D (4,6)-connected self-penetrating topology: the four-membered ring (red) is catenated by another four-membered ring (blue) and six-membered ring (green), respectively. (b) A 2D quadrate grid-like layer constructed from $[Mo_6O_{19}]^{4-}$ polyoxoanions and metal Ni^{2+} ions. (c) The three-dimensional framework of **71** along *b* axis.

Reproduced from Ref. [79] with permission from RSC© 2011.

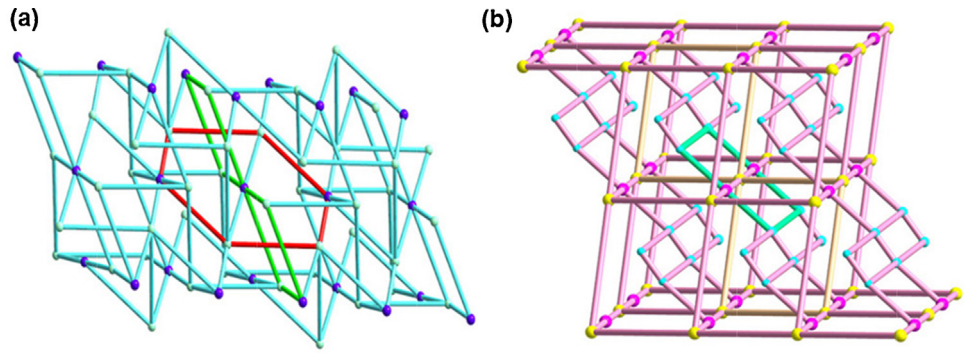

Fig. 16. (a) Topological representation of the (5,6)-connected framework of compound **74**. (b) Topological representation of the (4,6)-connected framework of compound **75**.
Reproduced from Ref. [34] with permission from Elsevier© 2011.

As shown in Scheme 1, the number of reported POM-based coordination polymers increases annually, however, the percentage of the entangled species in all POM-based coordination polymers seems to be relatively small. This maybe ascribed to the existence of the POMs. On one hand, a prerequisite of any entangled system is large pore spaces, but the relatively large nanoscale size of the POMs allows them to potentially block these voids to some extent, whether it acts as a linker or a template in the construction of the whole structure. On the other hand, the terminal oxygen atoms could also interact with the metal atoms or other polar molecules; like the formation of a hydrogen bond, all of these weak interactions may have a greater influence on the generation of the entanglement. Both of these characteristics may reduce the possibility of the entangled structures forming. However, it is just the special coordination ability and the high negative charges of the polyoxoanion, that enable metal atoms and organic ligands to coordinate in various ways, resulting in these novel and fascinating entangled features in this kind of coordination polymers.

6. Conclusion and outlook

Entangled POM-based coordination polymers, due to the various compositions and different coordination modes of POMs, have brought a variety of fresh examples for the entangled family. In this review, we have discussed recent efforts made toward understanding the structural features, rational syntheses of POM-based coordination polymers, and the roles of the POMs in the whole field of entangled structures. In the attempt to establish useful relationships between structures and properties for these species, different types of entanglement including interpenetration, polycatenanes, polyrotaxanes, poly*pseudo*-rotaxane and self-penetration have been discussed here. We have also attempted to make a detailed classification of every type of POM-based entangled structure based on the previous work in the literature and our own research results based on the dimensionalities of the individual components and the roles of the POMs in the framework.

Although a large number of POM-based coordination polymers with entangled structures have been synthesized, the development of this type of compound is still in its infancy. The exact formation mechanism of these structures is not yet clear and is usually ascribed to a self-assembly process, so controllable synthesis is a large challenge when designing and synthesizing POM-based coordination polymers with entangled structures. The study of the special properties of the corresponding entangled structure is extremely rare and the synthesis of special structures with targetable properties has not been achieved yet. The applied research of the POM-based coordination polymers with entangled structures, extending to the application research of POM-based coordination polymers remains to be further developed. Combining the advantages of the two components, attractive potential applications of the POMs and structure diversities of the entangled frameworks, the study of POM-based coordination polymers with entangled structures will be a sustainable research field in the coordination chemistry.

Acknowledgements

We are grateful to the editor for his kind invitation. The authors are pleased to acknowledge the fine work of the talented and dedicated graduate students, postdoctoral fellows, and colleagues who have worked with us in this area and whose names can be found in the references. This work was financially supported by Pre-973 Program (No. 2010CB635114), the National Natural Science Foundation of China (No. 21371099), the Science and Technology Department of Jiangsu Province for Distinguished Young Scholars (No. BK20130043), the program of Jiangsu Specially-Appointed Professor, the Natural Science Research of Jiangsu Higher Education Institutions (No. 13KJB150021) and the Foundation of Jiangsu Collaborative Innovation Center of Biomedical Functional Materials.

References

[1] (a) A. Müller, F. Peters, M.T. Pope, D. Gatteschi, Chem. Rev. 98 (1998) 239;
(b) C.-Y. Sun, S.-X. Liu, D.-D. Liang, K.-Z. Shao, Y.-H. Ren, Z.-M. Su, J. Am. Chem. Soc. 131 (2009) 1883;
(c) P. Putaj, F. Lefebvre, Coord. Chem. Rev. 255 (2011) 1642;
(d) B. Nohra, H. El Moll, L.M. Rodriguez Albelo, P. Mialane, J. Marrot, C. Mellot-Draznieks, M. O'Keeffe, R. Ngo Biboum, J. Lemaire, B. Keita, L. Nadjo, A. Dolbecq, J. Am. Chem. Soc. 133 (2011) 13363;
(e) A. Muller, P. Gouzerh, Chem. Soc. Rev. 41 (2012) 7431;
(f) H.N. Miras, J. Yan, D.-L. Long, L. Cronin, Chem. Soc. Rev. 41 (2012) 7403.
[2] S.G. Mitchell, C. Streb, H.N. Miras, T. Boyd, D.L. Long, L. Cronin, Nat. Chem. 2 (2010) 308.
[3] (a) L. Marleny Rodriguez-Albelo, A.R. Ruiz-Salvador, A. Sampieri, D.W. Lewis, A. Goímez, B. Nohra, P. Mialane, J.r.m. Marrot, F. Sécheresse, C. Mellot-Draznieks, R. Ngo Biboum, B. Keita, L. Nadjo, A. Dolbecq, J. Am. Chem. Soc. 131 (2009) 16078;
(b) H. Lv, Y.V. Geletii, C. Zhao, J.W. Vickers, G. Zhu, Z. Luo, J. Song, T. Lian, D.G. Musaev, C.L. Hill, Chem. Soc. Rev. 41 (2012) 7572;
(c) D.-L. Long, R. Tsunashima, L. Cronin, Angew. Chem. Int. Ed. 49 (2010) 1736;
(d) Y. Kikukawa, S. Yamaguchi, K. Tsuchida, Y. Nakagawa, K. Uehara, K. Yamaguchi, N. Mizuno, J. Am. Chem. Soc. 130 (2008) 5472.
[4] (a) D.A. Judd, J.H. Nettles, N. Nevins, J.P. Snyder, D.C. Liotta, J. Tang, J. Ermolieff, R.F. Schinazi, C.L. Hill, J. Am. Chem. Soc. 123 (2001) 886;
(b) D.-Y. Du, L.-K. Yan, Z.-M. Su, S.-L. Li, Y.-Q. Lan, E.-B. Wang, Coord. Chem. Rev. 257 (2013) 702;
(c) D.-Y. Du, J.-S. Qin, T.-T. Wang, S.-L. Li, Z.-M. Su, K.-Z. Shao, Y.-Q. Lan, X.-L. Wang, E.-B. Wang, Chem. Sci. 3 (2012) 705;
(d) D.-Y. Du, J.-S. Qin, C.-G. Wang, X.-C. Liu, S.-L. Li, Z.-M. Su, X.-L. Wang, Y.-Q. Lan, E.-B. Wang, J. Mater. Chem. 22 (2012) 21040;
(e) D.-Y. Du, J.-S. Qin, Y.-G. Li, S.-L. Li, Y.-Q. Lan, X.-L. Wang, K.-Z. Shao, Z.-M. Su, E.-B. Wang, Chem. Commun. 47 (2011) 2832.

[5] (a) A.J. Blake, N.R. Champness, P. Hubberstey, W.-S. Li, M.A. Withersby, M. Schröder, Coord. Chem. Rev. 183 (1999) 117;
(b) X.-M. Zhang, Coord. Chem. Rev. 249 (2005) 1201;
(c) F. Costantino, T. Bataille, N. Audebrand, E. Le Fur, C. Sangregorio, Cryst. Growth Des. 7 (2007) 1881;
(d) A.Y. Robin, K.M. Fromm, Coord. Chem. Rev. 250 (2006) 2127;
(e) J.-R. Li, Y. Tao, Q. Yu, X.-H. Bu, H. Sakamoto, S. Kitagawa, Chem. Eur. J. 14 (2008) 2771.
[6] (a) W. Kaneko, M. Mito, S. Kitagawa, M. Ohba, Chem. Eur. J. 14 (2008) 3481;
(b) A.K. Cheetham, C.N.R. Rao, R.K. Feller, Chem. Commun. (2006) 4780;
(c) S. Bauer, N. Stock, Angew. Chem. Int. Ed. 46 (2007) 6857;
(d) J. Li, W. Bi, W. Ki, X. Huang, S. Reddy, J. Am. Chem. Soc. 129 (2007) 14140;
(e) J. Zhang, S. Chen, H. Valle, M. Wong, C. Austria, M. Cruz, X. Bu, J. Am. Chem. Soc. 129 (2007) 14168.
[7] (a) X.-H. Bu, M.-L. Tong, H.-C. Chang, S. Kitagawa, S.R. Batten, Angew. Chem. Int. Ed. 43 (2004) 192;
(b) J.L.C. Rowsell, O.M. Yaghi, J. Am. Chem. Soc. 128 (2006) 1304.
[8] (a) V. Balzani, A. Credi, F.M. Raymo, J.F. Stoddart, Angew. Chem. Int. Ed. 39 (2000) 3348;
(b) V. Balzani, A. Credi, M. Venturi, Chem. Soc. Rev. 38 (2009) 1542.
[9] K. Liang, H. Zheng, Y. Song, M.F. Lappert, Y. Li, X. Xin, Z. Huang, J. Chen, S. Lu, Angew. Chem. Int. Ed. 43 (2004) 5776.
[10] Y.-H. Su, F. Luo, H. Li, Y.-X. Che, J.-M. Zheng, CrystEngComm 13 (2011) 44.
[11] L. Carlucci, G. Ciani, D.M. Proserpio, CrystEngComm 5 (2003) 269.
[12] C. Janiak, Dalton Trans. (2003) 2781.
[13] M.-L. Tong, X.-M. Chen, S.R. Batten, J. Am. Chem. Soc. 125 (2003) 16170.
[14] L. Carlucci, G. Ciani, D.M. Proserpio, Coord. Chem. Rev. 246 (2003) 247.
[15] S.R. Batten, R. Robson, Angew. Chem. Int. Ed. 37 (1998) 1460.
[16] S.R. Batten, CrystEngComm 3 (2001) 67.
[17] V.A. Blatov, L. Carlucci, G. Ciani, D.M. Proserpio, CrystEngComm 6 (2004) 378.
[18] W.L. Leong, J.J. Vittal, Chem. Rev. 111 (2010) 688.
[19] S.A. Bourne, J. Lu, B. Moulton, M.J. Zaworotko, Chem. Commun. (2001) 861.
[20] (a) I.A. Baburin, V.A. Blatov, L. Carlucci, G. Ciani, D.M. Proserpio, CrystEngComm 10 (2008) 1822;
(b) I.A. Baburin, V.A. Blatov, L. Carlucci, G. Ciani, D.M. Proserpio, J. Solid State Chem. 178 (2005) 2452.
[21] G.-P. Yang, L. Hou, X.-J. Luan, B. Wu, Y.-Y. Wang, Chem. Soc. Rev. 41 (2012) 6992.
[22] D.M. Proserpio, Nat. Chem. 2 (2010) 435.
[23] H.-L. Jiang, T.A. Makal, H.-C. Zhou, Coord. Chem. Rev. 257 (2013) 2232.
[24] J. Yang, J.-F. Ma, S.R. Batten, Chem. Commun. (2012) 7899.
[25] Y. Xu, G. Zhou, D. Zhu, Inorg. Chem. 47 (2007) 567.
[26] R.m. Dessapt, M. Collet, V. Coué, M. Bujoli-Doeuff, S.p. Jobic, C. Lee, M.-H. Whangbo, Inorg. Chem. 48 (2008) 574.
[27] H. Abbas, C. Streb, A.L. Pickering, A.R. Neil, D.-L. Long, L. Cronin, Cryst. Growth Des. 8 (2008) 635.
[28] (a) H. Abbas, A.L. Pickering, D.-L. Long, P. Kögerler, L. Cronin, Chem. Eur. J. 11 (2005) 1071;
(b) S. Upreti, A. Ramanan, Cryst. Growth Des. 5 (2005) 1837.
[29] (a) Y.-F. Song, H. Abbas, C. Ritchie, N. McMillian, D.-L. Long, N. Gadegaard, L. Cronin, J. Mater. Chem. 17 (2007) 1903;
(b) E.F. Wilson, H. Abbas, B.J. Duncombe, C. Streb, D.-L. Long, L. Cronin, J. Am. Chem. Soc. 130 (2008) 13876.
[30] Y.-M. Xie, R.-M. Yu, X.-Y. Wu, F. Wang, S.-C. Chen, C.-Z. Lu, CrystEngComm 12 (2010) 3490.
[31] H.-Y. Liu, H. Wu, J.-F. Ma, Y.-Y. Liu, J. Yang, J.-C. Ma, Dalton Trans. 40 (2011) 602.
[32] B.-X. Dong, Q. Xu, Inorg. Chem. 48 (2009) 5861.
[33] Y.-Q. Lan, S.-L. Li, X.-L. Wang, K.-Z. Shao, D.-Y. Du, H.-Y. Zang, Z.-M. Su, Inorg. Chem. 47 (2008) 8179.
[34] H.-Y. Zang, D.-Y. Du, S.-L. Li, Y.-Q. Lan, G.-S. Yang, L.-K. Yan, K.-Z. Shao, Z.-M. Su, J. Solid State Chem. 184 (2011) 1141.
[35] A.-X. Tian, J. Ying, J. Peng, J.-Q. Sha, Z.-M. Su, H.-J. Pang, P.-P. Zhang, Y. Chen, M. Zhu, Y. Shen, Cryst. Growth Des. 10 (2010) 1104.
[36] P. Zhang, J. Peng, X. Shen, Z. Han, A. Tian, H. Pang, J. Sha, Y. Chen, M. Zhu, J. Solid State Chem. 182 (2009) 3399.
[37] M.N. Sokolov, S.A. Adonin, E.V. Peresypkina, P.A. Abramov, A.I. Smolentsev, D.I. Potemkin, P.V. Snytnikov, V.P. Fedin, Inorg. Chim. Acta 394 (2013) 656.
[38] X.-L. Wang, D. Zhao, A.-X. Tian, G.-C. Liu, H.-Y. Lin, Y.-F. Wang, Q. Gao, X.-J. Liu, N. Li, Inorg. Chim. Acta 388 (2012) 114.
[39] A. Tian, J. Ying, X. Wang, J. Peng, Inorg. Chem. Commun. 14 (2011) 118.
[40] H. Yang, S. Gao, J. Lu□, B. Xu, J. Lin, R. Cao, Inorg. Chem. 49 (2010) 736.
[41] H. Yang, G. Li, B. Xu, T. Liu, Y. Li, R. Cao, S.R. Batten, Inorg. Chem. Commun. 12 (2009) 605.
[42] J. Liu, E. Wang, X. Wang, D. Xiao, L. Fan, J. Mol. Struct. 876 (2008) 206.
[43] Z. Zhang, J. Liu, Y. Li, S. Yao, E. Wang, X. Wang, J. Solid State Chem. 183 (2010) 228.
[44] L. Fan, D. Xiao, E. Wang, Y. Li, Z. Su, X. Wang, J. Liu, Cryst. Growth Des. 7 (2007) 592.
[45] S.-T. Zheng, G.-Y. Yang, Dalton Trans. 39 (2010) 700.
[46] Z. Shi, Z.-G. Kong, Q.-W. Wang, C.-B. Li, Inorg. Chem. Commun. 20 (2012) 131.
[47] X.-L. Wang, J. Li, A.-X. Tian, D. Zhao, G.-C. Liu, H.-Y. Lin, Cryst. Growth Des. 11 (2011) 3456.
[48] (a) P.-P. Zhang, J. Peng, H.-J. Pang, J.-Q. Sha, M. Zhu, D.-D. Wang, M.-G. Liu, Z.-M. Su, Cryst. Growth Des. 11 (2011) 2736;
(b) T. McGlone, C. Streb, M. Busquets-Fité, J. Yan, D. Gabb, D.-L. Long, L. Cronin, Cryst. Growth Des. 11 (2011) 2471;
(c) C. Streb, C. Ritchie, D.-L. Long, P. Kögerler, L. Cronin, Angew. Chem. Int. Ed. 46 (2007) 7579;
(d) C. Streb, R. Tsunashima, D.A. MacLaren, T. McGlone, T. Akutagawa, T. Nakamura, A. Scandurra, B. Pignataro, N. Gadegaard, L. Cronin, Angew. Chem. Int. Ed. 48 (2009) 6490;
(e) T. McGlone, C. Streb, D.-L. Long, L. Cronin, Adv. Mater. 22 (2010) 4275.
[49] H. Fu, Y. Lu, Z. Wang, C. Liang, Z.-M. Zhang, E.-B. Wang, Dalton Trans. 41 (2012) 4084.
[50] X.-F. Kuang, X.-Y. Wu, R.-M. Yu, J.P. Donahue, J.-S. Huang, C.-Z. Lu, Nat. Chem. 2 (2010) 461.
[51] Z. Shi, X. Gu, J. Peng, X. Yu, E. Wang, Eur. J. Inorg. Chem. (2006) 385.
[52] C.-J. Zhang, H.-J. Pang, Q. Tang, H.-Y. Wang, Y.-G. Chen, Dalton Trans. 39 (2010) 7993.
[53] X.-D. Du, C.-H. Li, Y. Zhang, S. Liu, Y. Ma, X.-Z. You, CrystEngComm 13 (2011) 2350.
[54] H. Wu, J. Yang, Y.-Y. Liu, J.-F. Ma, Cryst. Growth Des. 12 (2012) 2272.
[55] B. Liu, J. Yang, G.-C. Yang, J.-F. Ma, Inorg. Chem. 52 (2013) 84.
[56] X. Wang, H. Lin, Y. Bi, B. Chen, G. Liu, J. Solid State Chem. 181 (2008) 556.
[57] X. Wang, C. Xu, H. Lin, G. Liu, S. Yang, Q. Gao, A. Tian, CrystEngComm 14 (2012) 5836.
[58] H.-Y. Zang, Y.-Q. Lan, G.-S. Yang, X.-L. Wang, K.-Z. Shao, G.-J. Xu, Z.-M. Su, CrystEngComm 12 (2010) 434.
[59] X.-L. Wang, C. Qin, E.-B. Wang, Z.-M. Su, Chem. Commun. (2007) 4245.
[60] J.-X. Meng, Y. Lu, Y.-G. Li, H. Fu, E.-B. Wang, Cryst. Growth Des. 9 (2009) 4116.
[61] Y.-Q. Lan, S.-L. Li, Z.-M. Su, K.-Z. Shao, J.-F. Ma, X.-L. Wang, E.-B. Wang, Chem. Commun. (2008) 58.
[62] J.-H. Liao, J.-S. Juang, Y.-C. Lai, Cryst. Growth Des. 6 (2006) 354.
[63] Y.-Q. Lan, Li, X.-L. Wang, K.-Z. Shao, Z.-M. Su, E.-B. Wang, Inorg. Chem. 47 (2008) 529.
[64] C. Zhang, H. Pang, M. Hu, J. Li, Y. Chen, J. Solid State Chem. 182 (2009) 1772.
[65] B.-X. Dong, Q. Xu, Cryst. Growth Des. 9 (2009) 2776.
[66] X. Wang, X. Liu, A. Tian, J. Ying, H. Lin, G. Liu, J. Zhang, D. Zhao, Inorg. Chem. Commun. 17 (2012) 71.
[67] M. Zhu, S.-Q. Su, X.-Z. Song, Z.-M. Hao, S.-Y. Song, H.-J. Zhang, CrystEngComm 14 (2012) 6452.
[68] P.-P. Zhang, A.-X. Tian, J. Peng, H.-J. Pang, J.-Q. Sha, Y. Chen, M. Zhu, Y.-H. Wang, Inorg. Chem. Commun. 12 (2009) 902.
[69] (a) H.-J. Pang, J. Peng, C.-J. Zhang, Y.-G. Li, P.-P. Zhang, H.-Y. Ma, Z.-M. Su, Chem. Commun. 46 (2010) 5097;
(b) H.-J. Pang, H.-Y. Ma, J. Peng, C.-J. Zhang, P.-P. Zhang, Z.-M. Su, CrystEngComm 13 (2011) 7079.
[70] C. Qin, X.-L. Wang, E.-B. Wang, Z.-M. Su, Inorg. Chem. 47 (2008) 5555.
[71] X. Kuang, X.-Y. Wu, J. Zhang, C.-Z. Lu, Chem. Commun. (2011) 4150.
[72] Y.-Q. Lan, S.-L. Li, X.-L. Wang, K.-Z. Shao, D.-Y. Du, Z.-M. Su, E.-B. Wang, Chem. Eur. J. 14 (2008) 9999.
[73] A.-X. Tian, J. Ying, J. Peng, J.-Q. Sha, H.-J. Pang, P.-P. Zhang, Y. Chen, M. Zhu, Z.-M. Su, Cryst. Growth Des. 8 (2008) 3717.
[74] A.-X. Tian, X.-L. Lin, Y.-J. Liu, G.-Y. Liu, J. Ying, X.-L. Wang, H.-Y. Lin, J. Coord. Chem. 65 (2012) 2147.
[75] X.-L. Wang, Q. Gao, A.-X. Tian, H.-L. Hu, G.-C. Liu, J. Solid State Chem. 187 (2012) 219.
[76] X.-L. Wang, Q. Gao, A.-X. Tian, G.-C. Liu, Cryst. Growth Des. 12 (2012) 2346.
[77] A.-X. Tian, J. Ying, J. Peng, J.-Q. Sha, Z.-G. Han, J.-F. Ma, Z.-M. Su, N.-H. Hu, H.-Q. Jia, Inorg. Chem. 47 (2008) 3274.
[78] X.-L. Wang, D. Zhao, A.-X. Tian, J. Cluster Sci. 24 (2013) 259.
[79] G.-S. Yang, H.-Y. Zang, Y.-Q. Lan, X.-L. Wang, C.-J. Jiang, Z.-M. Su, L.-D. Zhu, CrystEngComm 13 (2011) 1461.
[80] C.-J. Zhang, H.-J. Pang, Q. Tang, H.-Y. Wang, Y.-G. Chen, New J. Chem. 35 (2011) 190.
[81] W.-Q. Kan, J. Yang, Y.-Y. Liu, J.-F. Ma, Inorg. Chem. 51 (2012) 11266.
[82] X. Wang, J. Li, A. Tian, G. Liu, Q. Gao, H. Lin, D. Zhao, CrystEngComm 13 (2011) 2194.